Intense two-week heatwave in Fennoscandia hotter and more likely due to climate change

Authors

Clair Barnes, *Centre for Environmental Policy, Imperial College, London, UK*
Ben Clarke, *Centre for Environmental Policy, Imperial College, London, UK*
Mika Rantanen*, Finnish Meteorological Institute, Helsinki, Finland*
Amalie Skålevåg, *Norwegian Meteorological Institute, Oslo, Norway*
Karianne Ødemark, *Norwegian Meteorological Institute, Oslo, Norway*
Erik Kjellström, *Rossby Centre, Swedish Meteorological and Hydrological Institute (SMHI), Norrköping, Sweden*
Maja Vahlberg, *Red Cross Red Crescent Climate Centre, The Hague, the Netherlands; Swedish Red Cross, Stockholm, Sweden (based in Ubmeje/Umeå, Sweden)*
Roop Singh, *Red Cross Red Crescent Climate Centre, The Hague, The Netherlands (based in New Jersey, USA)*
Friederike Otto, *Centre for Environmental Policy, Imperial College, London, UK*

Review authors

Mariam Zachariah, *Centre for Environmental Policy, Imperial College, London, UK*
Sarah Kew, *Royal Netherlands Meteorological Institute (KNMI), De Bilt, The Netherlands*
Claire Bergin, *Irish Climate Analysis Research Unit (ICARUS), Maynooth University, Ireland*
Dora Vrkić, *Grantham Institute - Climate Change and the Environment, Imperial College London, London, UK*
Lena B Hansson, *Swedish Red Cross, Stockholm, Sweden*
Tove Vikström, *Swedish Red Cross, Stockholm, Sweden*
Peter Hodgson, *Swedish Red Cross, Stockholm, Sweden*
Lotta Norberg, *Swedish Red Cross, Stockholm, Sweden*
Thea Holten, *Norwegian Red Cross, Oslo, Norway*
Suvi Virkkunen, *Finnish Red Cross, Helsinki, Finland*
Kirsti Kuusterä, *Finnish Red Cross, Helsinki, Finland*
Siru Aura, *Finnish Red Cross, Helsinki, Finland*
Paula Haro, *IFRC Regional Office for Europe, Budapest, Hungary*
Dalma Drobina, *IFRC Regional Office for Europe, Budapest, Hungary*
Hanna Sjölund, *Vision Trade Union, Stockholm, Sweden*

Report finalised: August 13th 2025

Main findings

- The July 2025 heatwave struck during the peak Nordic holiday season, leading to reduced staffing and strained healthcare, social services, and municipal functions across Norway, Sweden, and Finland. With formal, voluntary, and informal support systems under strain, response capacity was reduced, highlighting vulnerabilities in the care infrastructure during a period of growing climate extremes.
- This heatwave was unusual not only for its intensity but also for its duration, with multiple stations setting new records for consecutive days above 30°C and high temperatures lasting for more than two weeks. In today's climate, which has warmed globally by 1.3°C, the 14-day maximum temperatures in the study region observed in 2025 have a return time of about 50 years. The 14-day nighttime temperatures are less extreme in today's climate, with a return time of about 20 years. In a 1.3°C colder climate, however, such temperatures, day and night, would have been extremely rare.
- When combining the observation-based analysis with climate models to quantify the role of climate change in the 14-day heat event, we conclude that climate change made the extreme heat about 2°C hotter. The range of uncertainty for the change in likelihood of similar events is very wide because in many of the datasets (both in observations and climate models) the event would have been statistically impossible in a 1.3°C cooler climate, making it impossible to quantify. Based on the available evidence we conclude that similar events are at least ten times more likely to occur now than they would have been in a preindustrial climate without human-caused warming; however, this is likely an underestimate.
- In 2018, the region was hit by a similarly persistent heatwave. Due to warming increasing from 1.1 to 1.3°C, similar heatwaves are now estimated to be twice as likely as they were in 2018, when the region last experienced a prolonged heatwave. This finding highlights how even seemingly small increases in warming expose people to more frequent periods of dangerous heat.
- After a further 1.3°C of global warming – the level projected to be reached by the end of the century under current policies – the likelihood and intensity of such events are projected to continue to increase, becoming a further 1.7°C warmer and a further five times as likely.
- Nighttime temperatures have been made about 2°C hotter than they would have been without human-caused climate change, and around 33 times more likely. After a further 1.3°C of warming, nighttime temperatures are projected to warm by a further 1.7°C, with temperatures like those recorded in 2025 a further 7 times more likely to occur.
- Access to active cooling in Nordic homes is still limited but growing, mainly through heat pumps, which provide both heating and cooling. While these are now the main form of mechanical cooling, the 2018 heatwave showed that many buildings, including care facilities, and preschools, overheat in summer due to winter-focused design, often lacking both cooling systems and adequate shading. As heatwaves become more frequent, cold-focused building practices will need to be adjusted or supplemented with active cooling to avoid risks associated with indoor heat.

- Traditional Nordic summer activities such as staying in uninsulated cabins, camping, and alcohol consumption can increase heat-related risks due to limited cooling, physical strain, and dehydration, especially in remote areas. An increase in drowning deaths during the heat episode highlights additional risks that arise as people try to find ways to cool off.
- Climate extremes threaten Sámi livelihoods, with heat, drought, and forage shortages disrupting reindeer grazing and food access. Sámi leaders view these impacts as human rights issues and call for adaptation efforts that respect Indigenous rights and traditional knowledge.
- In addition to reindeer, high temperatures have additional impacts on the natural environment, including increasing tree cover loss, and incidences of harmful algal blooms which can impact aquatic ecosystems, recreation, and drinking water.
- Effective governance plays a crucial role in heat resilience, and while Nordic countries have strengthened risk assessments and institutional responsibilities since the 2018 heatwave, there are opportunities to strengthen coordination amongst municipal and private actors, and implement structural changes in care settings.

1 Introduction

After a relatively cool June, an exceptionally persistent heatwave affected Fennoscandia in July 2025, impacting Norway, Sweden and Finland. The heatwave event began on July 9th, when a high pressure system formed over the region. The orientation of the high was such that it allowed warm air masses to flow into Fennoscandia from the south and southeast, with large-scale subsidence and adiabatic warming elevating the temperatures further. In this air mass, 850 hPa temperatures exceeded +15°C, resulting in widespread 2-meter temperatures reaching or exceeding 30°C.

The July 2025 heatwave was particularly exceptional for its longevity, rather than its maximum temperatures. In Norway, two stations (Namsskogan and Gartland) in Trøndelag county set a new record for consecutive days above 30°C, with 13 days in a row. In Sweden, many stations recorded temperatures above 25°C for well over five days (the official heatwave threshold) during a 26 day period starting on the 9th. In the northern half of the country (Norrland), several stations registered at least 30°C on 13 consecutive days registered at least 30°C, starting on the 13th; long station records (Haparanda and Jokkmokk) indicate that there has not been a similarly long period of heatwave conditions in the last 100 years. Finland saw its longest streak of 30°C anywhere in the country, with 22 consecutive days reaching 30°C between 12 July and 2 August. In Ylitornio Meltosjärvi and Sodankylä Tähtelä, both located in Lapland, the daily maximum temperature reached over 25°C for 26 days in a row. This marks the longest streak of 25°C ever recorded in Finnish Lapland. Nighttime temperatures were also elevated during this period, with a number of stations across all three countries reporting one or more tropical nights (nighttime minimum temperature > 20°C). Figure 1.1 shows the daily maximum temperature anomalies with respect to the 1990-2020 July climatology, illustrating the persistence of the heatwave (daily minimum temperature anomalies in Figure A1.1).

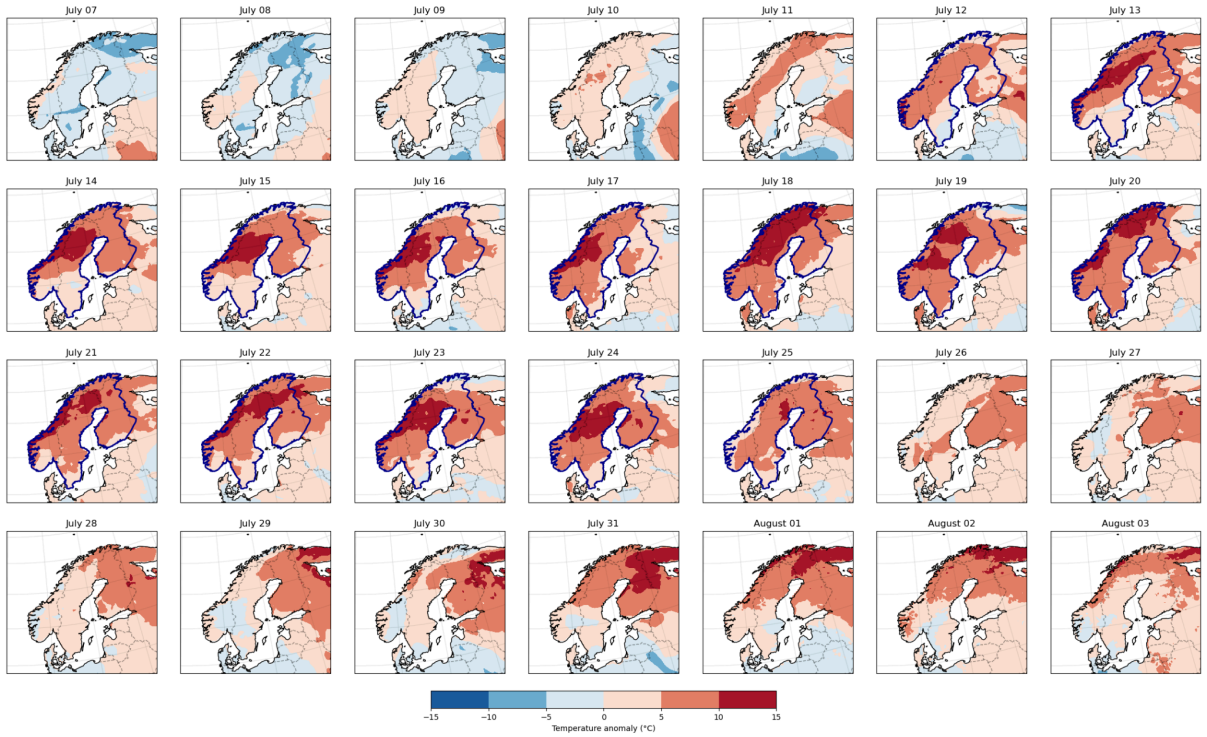

Figure 1.1: *Daily maximum temperature anomalies with respect to the 1990-2020 July climatology (ERA5). The study region is outlined in dark blue during the event period (hottest 14-day period averaged over the entire region).*

The weeks of heat caused a wide range of impacts. In Sweden, several people fainted during an outdoor play in Västernorrland, and numerous wildfires broke out and spread rapidly (TV4, 2025). At least 31 people drowned in July in the country (Sweden Herald, 2025). In Finland, emergency rooms in North Karelia were overcrowded with people suffering from heat-related issues, and the country saw a surge in drownings, with at least 11 recorded during the last weekend of July. Norway also reported an increase in hospitalisations (NRK, 2025) and drowning incidents (VG, 2025). The heat affected wildlife as well, with one particularly visible effect being reindeer, which are adapted to survive in cold weather, entering towns seeking to escape the heat and biting insects, and find water (Euronews, 2025; BBC, 2025). In Norway, drivers were warned about the danger of encountering them in tunnels as they fled the heat, and reindeer deaths were reported in Finland (Folkebladet, 2025; Itrosmo, 2025; RTE, 2025). Marine ecosystems were also impacted, with reports of algal blooms around the coastline making swimming hazardous (Finnish Environmental Institute, 17 July 2025).

1.1 Heatwaves in Fennoscandia

Heat extremes have increased across Fennoscandia in recent decades. In northern Fennoscandia, there has been a detectable increase in temperature extremes in the observational record since at least 1914. In Sweden, extremely warm months (defined as more than 3 standard deviations outside of the mean) have been more frequent in the last 30-year period compared to earlier in the observational record, which starts in 1860 (Joelsson et al., 2023). This increase is strongest in spring and autumn but is also

observable in summer (Kivinen et al., 2017). This pattern has been observed more broadly across all of Fennoscandia, with increasing seasonal maximum temperatures across all seasons, and the strongest increases in spring (Sulikowska & Wypych, 2021). This is matched by a strong increase of very severe extreme temperature events (defined as more than half of the region experiencing temperatures more than 2°C above the 95th percentile of seasonal temperatures) in the last 30 years, particularly in spring and summer (Sulikowska & Wypych, 2021). Similarly, using a large ensemble of seasonal hindcasts, significant positive increases have been found in 3-day extreme heat in early summer (May-July) across Scandinavia and Finland, which are strongest in central Sweden and Norway (Berghald et al., 2024).

Summer heatwaves in northern Europe, particularly in Fennoscandia, are typically driven by omega-blocking patterns interrupting the zonal flow of cool Atlantic air into the region (Zschenderlein et al., 2019, Kim et al. 2017). It is challenging to assess if, and how, such events are changing in a warming world. There is no clear evidence that summer blocking situations, such as those that occurred in 2018 and 2025, are becoming more frequent in Fennoscandia. Iles et al. (2025) found no robust trends in summer blocking over Scandinavia, and circulation analogue analysis likewise showed no statistically significant changes. These results suggest that the circulation patterns that led to persistent heatwaves in the summers of 2018 and 2025 can largely be attributed to internal atmospheric variability. However, analysis of an array of weather types across all seasons showed a systematic warming from the period 1961-1990 to the period 1991-2020, which implies that the observed changes cannot be explained by internal climate variability alone (Kjellström et al., 2022). This suggests that there is a robust and substantial thermodynamic influence of climate change on weather in the region.

In accordance with this, the observed trends are increasingly attributed to the warming climate. Working group 1 of the IPCC sixth assessment report reported that there is an increasing trend in heat extremes in northern Europe, and that this could be attributed with high confidence to human influence on the climate (Seneviratne et al., 2021). This result is based on a growing number of extreme event attribution studies.

In summer 2024, northern Fennoscandia experienced its warmest summer on record, and proxy-based reconstructions indicate that the summer was very likely the warmest summer in the region during the entire Common Era (Rantanen et al. 2024a). According to the same study, the average Jun-Aug temperature in 2024 was approximately 2.1°C higher due to human-induced climate change, making such an extreme event about 100 times more likely to occur now than in a pre-industrial climate.

In 2018, most of Europe experienced extreme summer heat, including much of Fennoscandia. Several attribution studies explored the human influence on this event in different locations and spatiotemporal scales. Over Scandinavia as a whole, the 1-day maximum temperatures in 2018 were found to be very rare even in the present climate, with return times of approximately 150 years. However, these would have been effectively impossible without the influence of human induced climate change (Leach et al., 2020). The most intense 10-day temperatures were also extreme over Scandinavia and had become nearly 200 times as likely due to human influence. While the whole region showed increasing trends in the 10-day maximum, the regionally aggregated probability ratio was increased by a very strong increase in temperatures in central Sweden (Leach et al., 2020). For Sweden specifically, anthropogenic climate change strongly increased the likelihood of a warm summer like 2018 as assessed across five different metrics, including average summer temperatures

and the number of heat days and events each year (Wilcke et al., 2020). Holmgren and Kjellström (2024) assessed that an event such as that observed in summer 2018 (more than 50 days with daily maximum temperatures above 25°C in an area covering much of southern Sweden) has become at least twice as probable due to man-made warming.

Another study considering 3-day maximum temperatures only at specific weather station locations found that stations in Sweden (Linköping), Finland (Sodankylä and Jokioinen) and Norway (Oslo Blindern) showed no clear trend with warming due to very high variability in summer extreme temperatures. However, this high variability was consistent with the large increases in likelihood found in analysis of large model ensembles, which showed statistically significant trends for individual grid cells containing those stations. The study therefore stated that human influence on the climate increased the likelihood of the observed heatwave in 2018, but did not quantify this change (World Weather Attribution, 2018). This finding was further corroborated in analysis of the regional temperatures over Scandinavia and Finland in a domain between 5°–30°E, 55°–70°N, which also found that these changes were driven largely by direct thermodynamic effects, rather than dynamical changes (Yiou et al., 2020). This study further found statistically significant increases in the probability of such events, with a probability ratio estimated between 5-2000, albeit with wide variations between model ensembles (Yiou et al., 2020).

To summarise, there is a clear increasing trend in extreme temperatures in Fennoscandia due to human influence on the climate. While extremes at the local scale exhibit high variability, changes in extremes at the regional and subregional scale are emerging strongly. As extremes with significant impacts continue to occur, event attribution studies at different spatiotemporal scales and temperature metrics can inform the changing hazards experienced by the region.

1.2 Event Definition

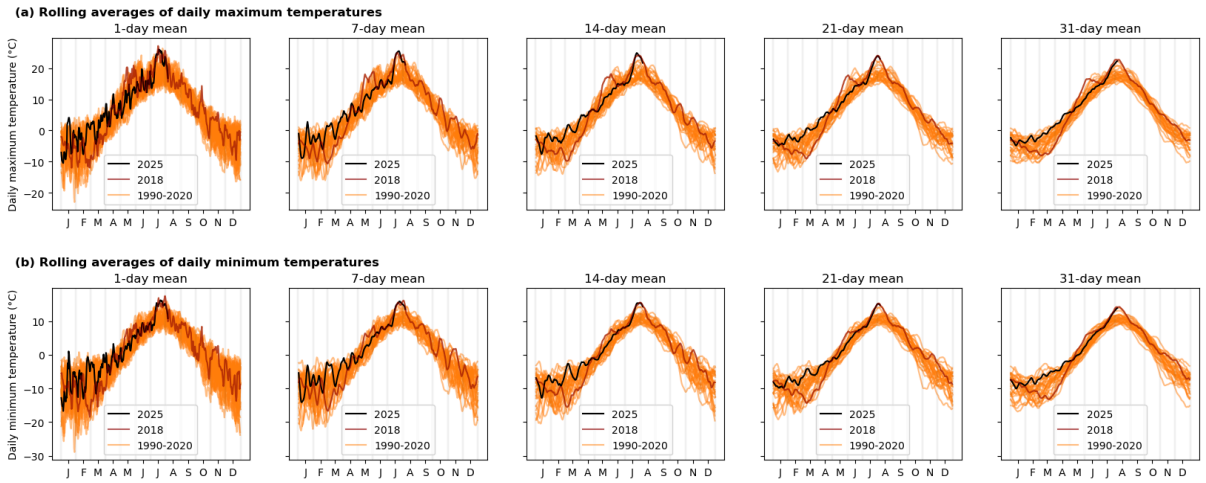

Figure 1.2: *Rolling n-day mean of (a) daily maximum temperatures and (b) daily minimum temperatures averaged over Fennoscandia. 2025 temperatures are in black, with 2018 in red for reference.*

The heatwave was remarkable both in its magnitude and its duration over the region, with both daily and night-time temperatures well above the average for the time of year (Figures 1.1 and 1.2). In order

to capture the spatial extent and persistence of the heatwave, we characterise it using two event definitions:

- **Tx14x** - annual maximum of 14-day averaged daily maximum temperatures, averaged over the contiguous region of mainland Norway, Sweden and Finland
- **Tn14x** - annual maximum of 14-day averaged daily minimum temperatures, averaged over the contiguous region of mainland Norway, Sweden and Finland

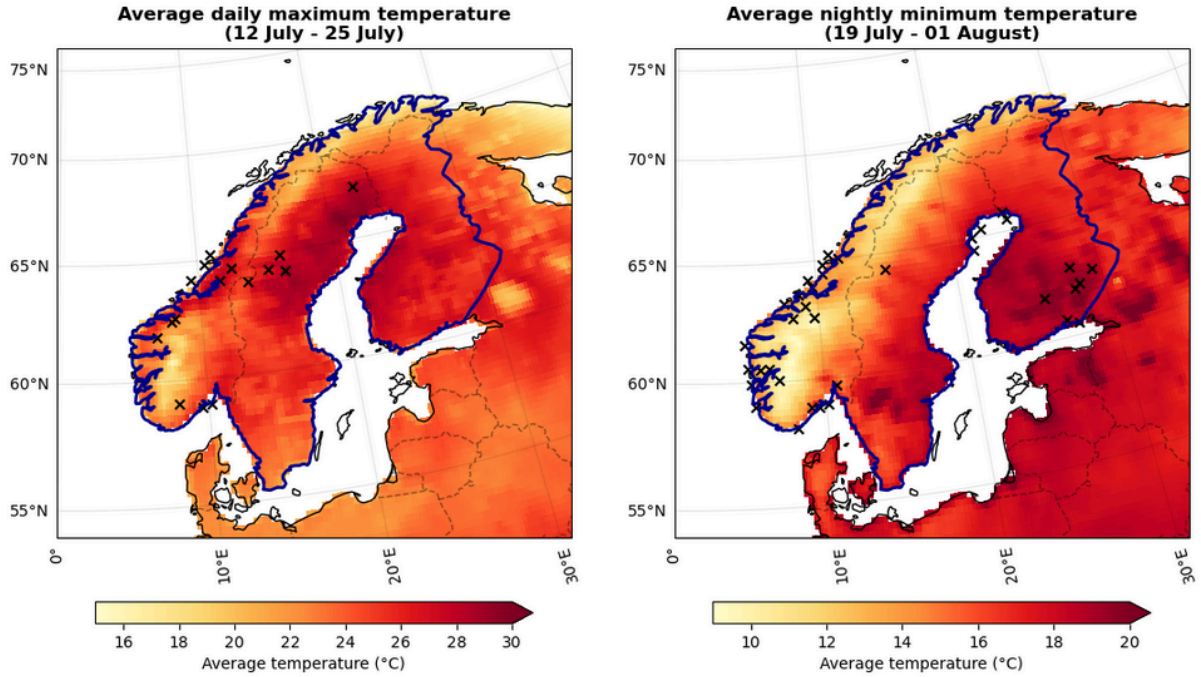

Figure 1.3: *Highest 14-day averaged daily maxima (left) and daily minima (right) over Fennoscandia. The study region is outlined in dark blue. Crosses mark sites where record temperatures were recorded.*

2 Data and methods

In this report, we study the influence of anthropogenic climate change on temperatures (characterised by Tx14x and Tn14x) in Norway, Sweden and Finland by comparing the likelihood and intensity of similar weather conditions at present with those in a 1.3°C cooler climate representing the preindustrial past (1850-1900, based on the Global Warming Index). We also extend this analysis into the future by assessing the influence of a further 1.3°C of global warming from present. This is in line with the latest Emissions Gap Report from the United Nations Environment Programme, which shows that the world is on track for at least 2.6°C temperature rise given currently implemented policies (UNEP, 2024).

2.1 Observational data

We first use observational and reanalysis data to estimate the return period of a similar event in the present day and to assess the historical trends. The observational datasets used are as follows:

- **ERA5** - The European Centre for Medium-Range Weather Forecasts's 5th generation reanalysis product, ERA5, is a gridded dataset that combines historical observations into global estimates using advanced modelling and data assimilation systems (Hersbach et al., 2020). We use daily maximum and minimum temperature data from this product at a resolution of 0.25° × 0.25°. Reanalysis data is available from January 1950 until the end of July 2025, supplemented with analysis data until August 6th.
- **E-OBS (v31.0e)** - This is a gridded land-only observation dataset of Europe, formed from the interpolation of station-derived meteorological observations (Cornes et al., 2018). We use daily maximum and minimum temperature data from this product at a resolution of 0.25° × 0.25°, from January 1920 to June 30th 2025.
- **CPC** - The CPC Global Unified Daily Temperature Dataset used for verification by NOAA/CPC, consisting of global GTS station data gridded to 0.5° × 0.5° resolution using the Shepheard algorithm (NOAA). This data is available from 1979 to near real time (August 9th). We use daily maximum and minimum temperatures from this dataset.

As a proxy for anthropogenic climate change we use the global mean surface temperature (GMST), where GMST is taken from the National Aeronautics and Space Administration (NASA) Goddard Institute for Space Science (GISS) surface temperature analysis (GISTEMP, Hansen et al., 2010 and Lenssen et al. 2019). To reduce variability in the GMST due to the El Nino-Southern Oscillation (ENSO), we use a four-year rolling average of the GMST, centred on the third year.

2.2 Model and experiment descriptions

We use two multi-model ensembles from climate modelling experiments using very different framings (Philip et al., 2020): coupled global circulation models (CMIP6) and regional climate models (Euro-CORDEX).

- **CMIP6** - this is a multi-model ensemble of global general circulation models with varying resolutions (Eyring et al., 2016). For all simulations, the period 1850 to 2015 is based on historical simulations, while the SSP5-8.5 scenario is used to project from 2016 to 2070. We use 32 of the participating models (see Tables 5.1 and 5.2 for details).
- **Euro-CORDEX** - the Coordinated Regional Climate Downscaling Experiment (CORDEX)-European Domain at 0.11° resolution (EUR-11, Jacob et al., 2014; Vautard et al., 2021). The ensemble consists of 50 runs from a combination of twelve regional climate models (RCMs) with boundary conditions from eight GCMs from the CMIP5 ensemble (see Tables 5.1 and 5.2 for details). These simulations are composed of historical simulations from 1950 or 1970 up to 2005, and extended to the year 2100 using the RCP8.5 scenario.

2.3 Statistical methods

Methods for observational and model analysis and for model evaluation and synthesis are used according to the World Weather Attribution Protocol, described in Philip et al., (2020), with

supporting details found in van Oldenborgh et al., (2021), Ciavarella et al., (2021), Otto et al., (2024) and here. The key steps, presented in sections 3-6, are: (3) trend estimation from observations; (4) model validation; (5) multi-method multi-model attribution; and (6) synthesis of the attribution statement.

For each time series we estimate the parameters of a statistical model in which the index depends on the GMST. This model is then used to estimate the return period and intensity of the event under study for the 2025 GMST and for a 1.3°C cooler counterfactual climate: this allows us to compare the expected intensity and frequency of similar events now and in the preindustrial past (1850-1900, based on the Global Warming Index), by calculating the probability ratio (PR; the factor-change in the event's probability) and change in intensity of the event.

A nonstationary GEV distribution is used to model both Tx14x and Tn14x. In each case, the distribution is assumed to shift linearly with the GMST covariate, while the variance remains constant. The parameters of the statistical model are estimated using maximum likelihood.

3 Observational analysis: return period and trend

3.1 Tx14x

Figure 3.1 shows the time series of Tx14x (annual maxima of 14-day average of daily maximum temperatures averaged over Fennoscandia) in three gridded data products, with the fitted GMST-dependent trend overlaid. The GMST-dependent trend (black line) closely resembles the nonparametric local regression (Loess) smoother fitted over time (green line), suggesting that the fitted model captures the temporal trend well. All three datasets show a clear upward trend in 14-day maximum temperatures; while E-Obs did not cover the event at the time of writing, the 2025 heatwave is the highest recorded in both ERA5 and CPC, lying close to or above the upper blue line that represents the expected magnitude of a once-in-40-year event. In ERA5, the event has a return period of 76 years (bootstrapped 95% confidence interval: 19 years, infinite) and in CPC, 33 years (95% interval: 7 years, infinite). We therefore use a return period of 50 years to represent this event in the full attribution analysis.

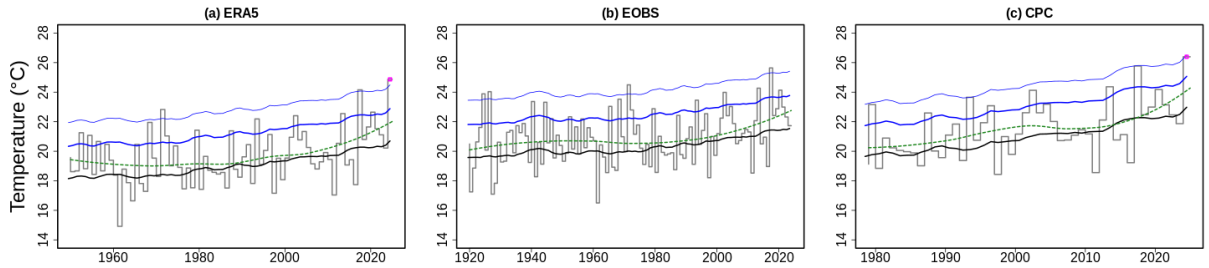

Figure 3.1: *Time series of Tx14x over Fennoscandia, with fitted model overlaid. The pink dot marks the 2025 event (not yet available in E-Obs); the heavy black line indicates the mean of the fitted GEV model, and the blue lines indicate the expected return levels of 6- and 40-year events. The green line is a nonparametric Loess smoother.*

Figure 3.2 shows the fitted linear trend plotted against the GMST covariate, rather than time as above. In ERA5 the hottest 14-day period in Fennoscandia is found to have warmed by 2.6°C (95% confidence interval: 1.0, 4.2) with respect to the preindustrial baseline; in E-Obs, by 2.0°C (95% confidence interval: 0.7, 3.3). In CPC the fitted trend is stronger, with Tx14x warming by an estimated 4.4°C (95% confidence interval: 1.8, 6.9). This stronger trend is due to the fact that CPC only covers the satellite era from 1979 onwards; in a sensitivity analysis not shown here, trends fitted to the same period in ERA5 and E-Obs were of similar magnitude, suggesting that the rate of warming has increased in recent decades, possibly due to changes in snow cover (Kivinen et al., 2017; Rantanen et al., 2024b), and in line with the period of rapid Arctic warming (Rantanen et al., 2022). For this reason, we exclude the CPC results from the hazard synthesis in section 6. However, we note that both CPC and E-Obs are derived from station data and where they overlap, the two time series of Tx14x are almost identical, so we are not losing any information through this omission.

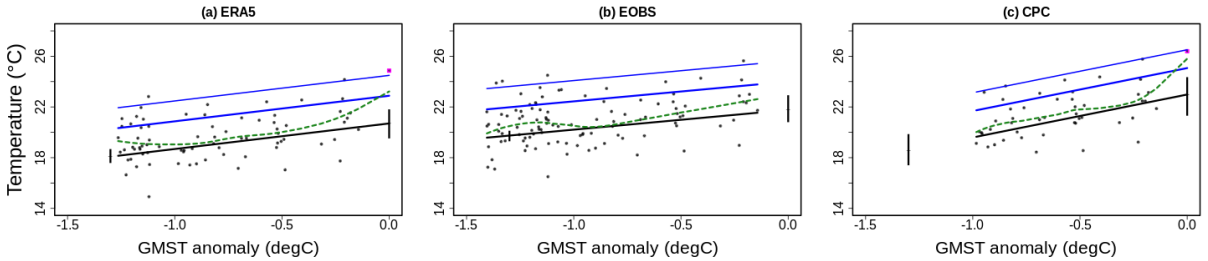

Figure 3.2: *Linear trend in Tx14x over Fennoscandia as a function of GMST (shown as a difference from the 2025 GMST) in three gridded observational data products. The pink dot marks the 2025 event (not yet available in E-Obs); the thick black line denotes the nonstationary location of the fitted GEV distribution, and the blue lines show estimated 6- and 40-year return levels. The vertical lines represent a bootstrapped 95% confidence interval for the GEV location parameter in the 2025 climate (GMST anomaly = 0) and a hypothetical 1.3°C cooler climate. The 2025 observation is highlighted in magenta.*

Figure 3.3 shows the modelled change in return levels associated with a 1.3°C increase in GMST from the preindustrial to the current climate. In all three panels, the points representing the temperatures actually recorded in each dataset lie close to the lines representing the expected values, indicating that the statistical model represents the distribution of the data well. In all datasets, there is a clear separation between the return levels in the current climate (red) and the past climate (blue); in both ERA5 and CPC, the pink dashed line representing the temperature of the observed event (pink dashed line) does not intersect with the blue line, indicating that, according to the model, an event of this magnitude would have been essentially impossible in a preindustrial climate. Because of this, the best estimate of the probability ratio - that is, the factor change in the probability of such an event occurring - is infinite in both datasets, while in E-Obs, a hypothetical 50-year event is now estimated to be 1300 times more likely now than in a preindustrial climate. These results, along with the estimated return periods and changes in intensity for all datasets, are summarised in Table 3.1.

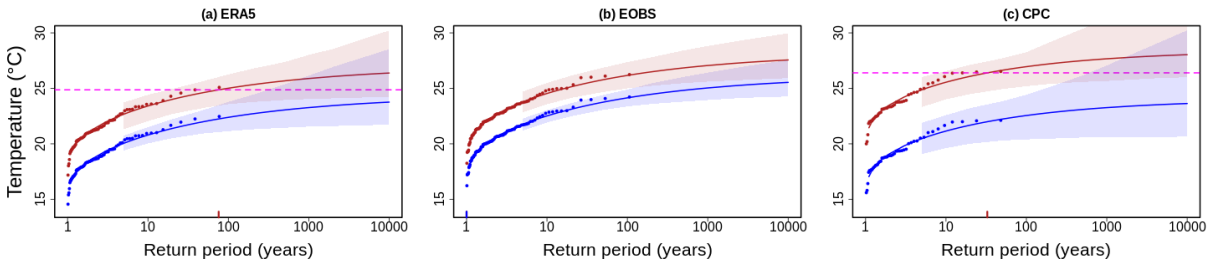

Figure 3.3: *Expected return levels of Tx14x over the study region in the 2025 climate (red lines) and in a 1.3°C cooler counterfactual climate (blue line), estimated from the statistical model described in section 2.3. Shaded regions represent 95% confidence intervals obtained via a bootstrapping procedure. The pink line shows the 14-day average temperature observed during July 2025 (not yet available in E-Obs). Red and blue ticks at the x axis indicate the estimated return level of the event in the 2025 climate and counterfactual climate.*

	Observed Tx14x (°C)	Return period (years)	Change in intensity (°C)	Probability ratio
ERA5	24.9	75.8 (18.6, Inf)	**2.62 (1.01, 4.21)**	**Inf (3.86, Inf)**
E-Obs	-	50	**2.02 (0.732, 3.27)**	**1300 (6.42, Inf)**
CPC	26.4	32.6 (7.2, Inf)	**4.4 (1.82, 6.94)**	**Inf (14.7, Inf)**

Table 3.1: *Summary of fitted model results for Tx14x: event magnitude; return period of 2025 Tx14x in the 2025 climate; change in Tx14x and factor change in likelihood (probability ratio) associated with 1.3°C of global warming. Figures in parenthesis indicate 95% confidence interval obtained via bootstrapping. Statistically significant changes are highlighted in* ***bold****.*

3.1.1. Changes in Tx14x since 2018

Parallels have been drawn between the 2025 heatwave and a heatwave in 2018 that reached similar temperatures for a prolonged period over most of Norway, Sweden and Finland. The fitted statistical model allows us to estimate the temperature and return period of the hottest two-week period in the study region in 2018, and also to estimate the observed change in intensity and likelihood associated with the 0.2°C of global warming that has occurred in the intervening seven years (Table 3.2). All three datasets agree that the event was almost as extreme as the 2025 event, with an estimated return period of between 37 and 69 years. In the longer ERA5 and E-Obs time series, the hottest 14-day periods are now an estimated 0.3 - 0.4°C warmer, and events as extreme as the 2018 heatwave are almost twice as likely to occur in 2025 as they were in 2018. The trends in the shorter CPC time series are stronger, with a temperature increase of 0.7°C and similar events now almost three times as likely to occur; however, since (as noted above) it is unclear whether this short-term trend actually reflects the direct effects of climate change, we report the lower figures from the longer time series as a more robust but probably conservative estimate.

	Observed Tx14x (°C)	2018 return period (years)	Change in intensity (°C)	Probability ratio
ERA5	24.2	45.9 (14.9, Inf)	**0.42 (0.133, 0.67)**	**1.87 (1.18, 81.11)**
E-Obs	25.6	68.8 (20.6, 3200)	**0.324 (0.14, 0.533)**	**1.71 (1.3, 3.73)**
CPC	25.8	37.6 (13.8, Inf)	**0.706 (0.305, 1.087)**	**2.88 (1.45, 35.51)**

Table 3.2: *Summary of fitted model results for 2018 Tx14x: event magnitude; return period of 2018 Tx14x in the 2018 climate; change in Tx14x and factor change in likelihood (probability ratio) associated with 0.2°C of*

global warming from 2018 to 2025. Figures in parenthesis indicate 95% confidence interval obtained via bootstrapping. Statistically significant changes are highlighted in ***bold****.*

3.2 Tn14x

Figure 3.4 shows the time series of Tn14x (annual maxima of 14-day average of daily minimum temperatures averaged over Fennoscandia) in three gridded data products, with the fitted GMST-dependent trend overlaid. From around 1960 onwards the GMST-dependent trend (black line) closely resembles the nonparametric local regression (Loess) smoother fitted over time (green line), suggesting that the fitted model captures the temporal trend well in this period; however, the 1920s-1950s are somewhat warmer than predicted by the model in E-Obs, suggesting that there may be some other factor influencing trends in daily minima in this region that is not captured by the model, which will increase uncertainty in the final results. Despite this, all three datasets show a clear upward trend in 14-day minimum temperatures, with no apparent acceleration of the rate of warming in recent decades. In terms of nightly temperatures, the 2025 heatwave was the second warmest two-week period recorded in ERA5 but was less extreme in CPC. In ERA5, the event has a return period of 27 years (bootstrapped 95% confidence interval: 9 to 236 years) and in CPC, 9 years (95% interval: 3 to 112 years). We therefore use a return period of 20 years to represent this event in the full attribution analysis.

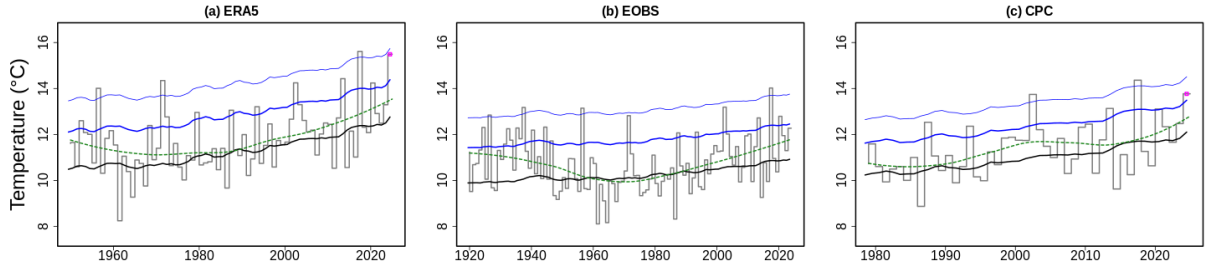

Figure 3.4: *Time series of Tn14x over Fennoscandia, with fitted model overlaid. The pink dot marks the 2025 event (not yet available in E-Obs); the heavy black line indicates the mean of the fitted GEV model, and the blue lines indicate the expected return levels of 6- and 40-year events. The green line is a nonparametric Loess smoother.*

Figure 3.5 shows the fitted linear trend plotted against the GMST covariate, rather than time as above. In ERA5, the warmest 14-night period in Fennoscandia is found to have warmed by 2.3°C (95% confidence interval: 1.1, 3.5) with respect to the preindustrial baseline; in E-Obs, which includes more of the warmer period prior to 1960, by 1.1°C (95% confidence interval: 0.2, 1.8); in CPC, by 2.5°C (0.4, 4.3). Again, when using only data from 1979 onwards we see very similar fitted trends in E-Obs and CPC, which are both based on station data; we therefore again exclude CPC from the hazard synthesis to avoid biasing the results toward recent trends.

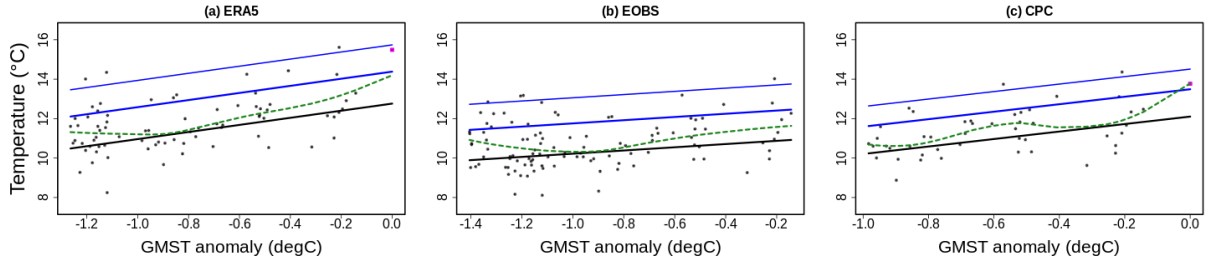

Figure 3.5: *Linear trend in Tn14x over Fennoscandia as a function of GMST (shown as a difference from the 2025 GMST) in three gridded observational data products. The pink dot marks the 2025 event (not yet available in E-Obs); the thick black line denotes the nonstationary location of the fitted GEV distribution, and the blue lines show estimated 6- and 40-year return levels. The vertical lines represent a bootstrapped 95% confidence interval for the GEV location parameter in the 2025 climate (GMST anomaly = 0) and a hypothetical 1.3°C cooler climate. The 2025 observation is highlighted in magenta.*

Figure 3.6 shows the modelled change in return levels associated with a 1.3°C increase in GMST from the preindustrial to the current climate. In all three panels, the points representing the temperatures actually recorded in each dataset lie close to the lines representing the expected values, indicating that the statistical model represents the distribution of the data well. In ERA5 and CPC, there is a clear separation between the return levels in the current climate (red) and the past climate (blue), while in E-Obs the two confidence intervals are adjacent even at their narrowest. In CPC, the pink dashed line representing the temperature of the observed event (pink dashed line) does not intersect with the blue line, indicating that according to the model, an event of this magnitude would have been essentially impossible in a preindustrial climate, and resulting in an infinite best estimate of the probability ratio. In ERA5, the probability ratio (the factor change in likelihood of an event of the observed temperature) is estimated to be 538 (95% confidence interval: 4.18, infinite) and in E-Obs, to be 7.3 (95% confidence interval: 1.39, infinite). These results, along with the estimated return periods and changes in intensity for all datasets, are summarised in Table 3.3.

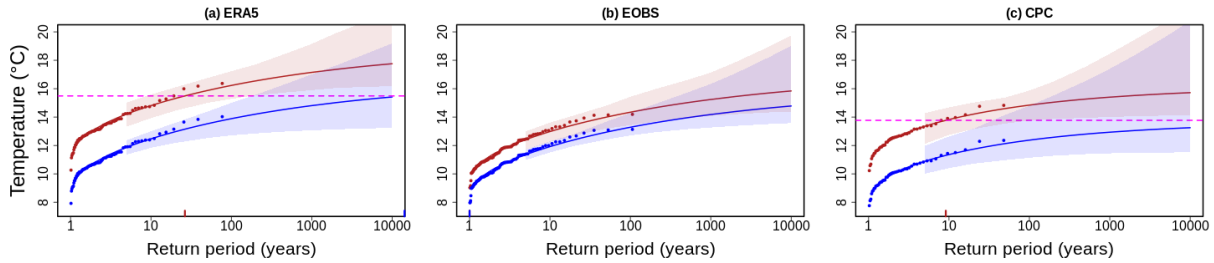

Figure 3.6: *Expected return levels of Tn14x over the study region in the 2025 climate (red lines) and in a 1.3°C cooler counterfactual climate (blue line), estimated from the statistical model described in section 2.3. Shaded regions represent 95% confidence intervals obtained via a bootstrapping procedure. The pink line shows the 14-day average nightly minimum temperature observed during July 2025 (not yet available in E-Obs). Red and blue ticks at the x axis indicate the estimated return level of the event in the 2025 climate and counterfactual climate.*

	Observed Tn14x (°C)	**Return period (years)**	**Change in intensity (°C)**	**Probability ratio**
ERA5	15.5	26.5 (8.64, 236)	**2.34 (1.12, 3.51)**	**538 (4.18, Inf)**

E-Obs	-	20 (8.61, 132)	**1.06 (0.158, 1.84)**	**7.3 (1.39, 140)**
CPC	13.8	9.12 (2.65, 112)	**2.47 (0.353, 4.26)**	**Inf (1.49, Inf)**

Table 3.3: *Summary of fitted model results for Tn14x: event magnitude; return period of 2025 Tn14x in the 2025 climate; change in Tn14x and factor change in likelihood (probability ratio) associated with 1.3°C of global warming. Figures in parenthesis indicate 95% confidence interval obtained via bootstrapping. Statistically significant changes are highlighted in* ***bold****.*

4 Model evaluation

The climate models are evaluated against the observational data products for their ability to capture the seasonal cycle of daily maximum and minimum temperature over the study region. Models are considered 'good' if they recreate the full seasonal cycle; 'reasonable' if they replicate spring trends faithfully; and 'bad' if the spring cycle is not well represented. We also evaluate the models in terms of how well they replicate observed large-scale spatial patterns of maximum and minimum daily temperatures over Sweden, Norway and Finland.

We then evaluate the model in terms of how well they replicate the distribution of the class of events in question, by evaluating how well the scale and shape parameters of the fitted statistical model match those estimated from the observational datasets. For each parameter, a model is labelled as 'good' if the best estimate of each parameter falls within the bounds estimated from the observations; 'reasonable' if the confidence interval for the model overlaps with the range estimated from the observations; or 'bad' if the ranges do not overlap.

If a model is 'good' for all criteria, we give it an overall rating of 'good'; we rate the model as 'reasonable' or 'bad', if it is rated 'reasonable' or 'bad', respectively, for at least one criterion. For each framing/ensemble we aim to use only models that are classified as 'good', but if five or fewer models from that framing/ensemble perform well, we also use models that only just pass the evaluation tests. Where multiple versions of the same model pass the evaluation, we retain the highest-resolution version or, if all runs have the same resolution, the lowest-numbered version, with the remainder flagged as 'duplicate' in the table below. We also exclude any models for which the best estimate of the probability ratio is infinite, flagging these as 'inf_pr' in the tables.

Tables 4.1 and 4.2 show the results of the model validation for Tx14x and Tn14x over the study region. All models deemed 'good' were included in the final analysis. Plots comparing the seasonal cycle for each model with the observed seasonal cycles can be found in Figures A2.1 - A2.6.

Table 4.1: *Evaluation of the climate models considered for attribution of Tx14x over Fennoscandia. For each model, the best estimate of the scale and shape parameters is shown, along with a 95% confidence obtained via bootstrapping. The overall evaluation is shown in the right-hand column; only models receiving a category of 'good' overall were included in the final analysis.*

Observations / models	Seasonal	Spatial	Scale parameter	Shape parameter	Overall
ERA5			1.58 (1.2, 1.87)	-0.25 (-0.44, -0.05)	

EOBS			1.61 (1.34, 1.84)	-0.25 (-0.38, -0.13)	
CPC			1.55 (1, 1.92)	-0.28 (-0.57, 0.05)	
ACCESS-CM2_r1	good	good	1.73 (1.37, 2.01)	-0.22 (-0.38, -0.05)	good
ACCESS-ESM1-5_r1	reasonable	reasonable	1.4 (1.09, 1.62)	-0.11 (-0.28, 0.11)	reasonable
AWI-CM-1-1-MR_r1	reasonable	good	1.76 (1.39, 2.03)	-0.17 (-0.38, 0.03)	reasonable
BCC-CSM2-MR_r1	bad	bad	1.29 (0.03, 2.19)	0.96 (-0.19, 3.12)	bad
CMCC-ESM2_r1	reasonable	reasonable	1.72 (1.42, 1.98)	-0.26 (-0.41, -0.08)	reasonable
CNRM-CM6-1_r1	good	good	1.47 (1.19, 1.82)	-0.34 (-0.68, -0.12)	good
CNRM-CM6-1-HR_r1	good	good	1.42 (1.12, 1.66)	-0.25 (-0.51, -0.11)	inf_pr
EC-Earth3_r1	good	good	1.65 (1.3, 1.89)	-0.06 (-0.19, 0.13)	good
EC-Earth3-CC_r1	good	good	1.75 (1.34, 2.07)	-0.15 (-0.29, 0.08)	good
EC-Earth3-Veg-LR_r1	good	good	1.5 (1.21, 1.78)	-0.17 (-0.41, 0.03)	good
FGOALS-g3_r1	reasonable	reasonable	1.73 (1.41, 1.99)	-0.24 (-0.43, -0.13)	reasonable
GFDL-CM4_r1	good	good	1.18 (1, 1.33)	-0.18 (-0.44, -0.04)	good
GFDL-CM4_r2	good	reasonable	1.17 (1, 1.33)	-0.18 (-0.44, -0.04)	reasonable
GFDL-ESM4_r1	good	good	1.39 (1.17, 1.62)	-0.46 (-0.67, -0.3)	inf_pr
HadGEM3-GC31-LL_r1	good	good	1.44 (1.17, 1.67)	-0.21 (-0.42, -0.08)	good
INM-CM4-8_r1	reasonable	reasonable	1.3 (1.04, 1.52)	-0.19 (-0.37, -0.01)	reasonable
INM-CM5-0_r1	reasonable	reasonable	1.12 (0.9, 1.32)	0.02 (-0.15, 0.19)	reasonable
IPSL-CM6A-LR_r1	good	good	1.6 (1.33, 1.86)	-0.36 (-0.65, -0.2)	good
KACE-1-0-G_r1	reasonable	reasonable	2.3 (1.91, 2.69)	-0.19 (-0.42, -0.03)	reasonable
KIOST-ESM_r1	reasonable	good	1.01 (0.85, 1.16)	-0.03 (-0.31, 0.13)	reasonable
MPI-ESM1-2-LR_r1	reasonable	good	1.17 (0.97, 1.35)	-0.06 (-0.28, 0.07)	reasonable
MRI-ESM2-0_r1	bad	good	1.34 (1.09, 1.54)	-0.23 (-0.43, -0.07)	bad
NESM3_r1	good	good	1.62 (1.39, 1.84)	-0.22 (-0.47, -0.04)	good
NorESM2-LM_r1	bad	good	1.53 (1.11, 1.81)	-0.15 (-0.3, 0.05)	inf_pr
TaiESM1_r1	bad	good	2.15 (1.81, 2.46)	-0.26 (-0.53, -0.16)	bad
CanESM2_r1_CCLM4-8-17	good	good	1.75 (1.37, 2.08)	-0.12 (-0.26, 0.06)	good
CanESM2_r1_REMO2015	good	good	1.88 (1.44, 2.19)	-0.22 (-0.35, -0.05)	good
CNRM-CM5_r1_ALADIN63	good	good	1.58 (1.28, 1.82)	-0.28 (-0.44, -0.16)	good
CNRM-CM5_r1_CCLM4-8-17	good	good	1.69 (1.38, 2.05)	-0.25 (-0.5, -0.08)	good
CNRM-CM5_r1_HadREM3-GA7-05	good	good	3.57 (1.08, 5)	-0.54 (-0.83, 0.17)	inf_pr
CNRM-CM5_r1_HIRHAM5	good	good	1.39 (1.15, 1.59)	-0.21 (-0.37, -0.05)	good
CNRM-CM5_r1_RACMO22E	good	good	1.54 (1.26, 1.76)	-0.07 (-0.22, 0.09)	good
CNRM-CM5_r1_RCA4	reasonable	good	1.25 (0.97, 1.54)	-0.09 (-0.32, 0.2)	reasonable
CNRM-CM5_r1_REMO2015	good	good	1.51 (1.22, 1.76)	-0.16 (-0.35, 0.05)	good
EC-EARTH_r12_CCLM4-8-17	good	good	1.79 (1.37, 2.15)	-0.19 (-0.34, 0.01)	inf_pr
EC-EARTH_r12_COSMO-crCLIM-v1-1	good	good	1.22 (0.92, 1.41)	-0.11 (-0.29, 0.08)	duplicate
EC-EARTH_r12_HadREM3-GA7-05	good	good	3.31 (1.1, 4.51)	-0.66 (-0.91, 0.23)	inf_pr

EC-EARTH_r12_HIRHAM5	good	good	1.49 (1.19, 1.75)	-0.23 (-0.48, -0.08)	duplicate
EC-EARTH_r12_RACMO22E	reasonable	good	1.57 (1.12, 1.92)	-0.13 (-0.39, 0.18)	duplicate
EC-EARTH_r12_RCA4	reasonable	good	1.22 (0.78, 1.51)	-0.2 (-0.36, 0.16)	reasonable
EC-EARTH_r12_RegCM4-6	good	good	1.32 (0.98, 1.6)	-0.19 (-0.42, 0.05)	good
EC-EARTH_r12_REMO2015	good	good	1.56 (1.31, 1.85)	-0.11 (-0.43, 0.04)	good
EC-EARTH_r12_WRF361H	reasonable	good	1.34 (0.95, 1.76)	-0.19 (-0.61, 0.14)	reasonable
EC-EARTH_r1_COSMO-crCLIM-v1-1	good	good	1.37 (1.1, 1.59)	-0.07 (-0.22, 0.08)	good
EC-EARTH_r1_HIRHAM5	good	good	1.44 (1.18, 1.65)	-0.24 (-0.38, -0.1)	good
EC-EARTH_r1_RACMO22E	good	good	1.64 (1.38, 1.9)	-0.38 (-0.6, -0.23)	inf_pr
EC-EARTH_r1_RCA4	reasonable	good	1.15 (0.91, 1.35)	-0.27 (-0.45, -0.08)	inf_pr
EC-EARTH_r3_COSMO-crCLIM-v1-1	good	good	1.73 (1.46, 1.94)	-0.29 (-0.48, -0.15)	duplicate
EC-EARTH_r3_HIRHAM5	good	good	1.56 (1.25, 1.8)	-0.32 (-0.53, -0.11)	inf_pr
EC-EARTH_r3_RACMO22E	good	good	1.73 (1.42, 1.95)	-0.22 (-0.34, -0.07)	good
EC-EARTH_r3_RCA4	reasonable	good	1.09 (0.69, 1.38)	0.07 (-0.19, 0.52)	reasonable
HadGEM2-ES_r1_ALADIN63	good	good	1.57 (1.23, 1.83)	-0.19 (-0.47, 0.04)	good
HadGEM2-ES_r1_CCLM4-8-17	good	good	1.46 (1.16, 1.71)	-0.1 (-0.33, 0.1)	inf_pr
HadGEM2-ES_r1_COSMO-crCLIM-v1-1	good	good	1.31 (1.09, 1.54)	-0.2 (-0.41, 0)	good
HadGEM2-ES_r1_HIRHAM5	good	good	1.37 (1.08, 1.66)	-0.16 (-0.46, 0.07)	good
HadGEM2-ES_r1_RACMO22E	good	good	1.61 (1.33, 1.87)	-0.16 (-0.34, 0.05)	good
HadGEM2-ES_r1_RCA4	good	good	1.33 (1.05, 1.61)	-0.22 (-0.59, -0.06)	good
HadGEM2-ES_r1_RegCM4-6	good	good	1.33 (0.97, 1.56)	-0.07 (-0.27, 0.18)	good
HadGEM2-ES_r1_REMO2015	good	good	1.4 (1.15, 1.61)	-0.29 (-0.42, -0.15)	inf_pr
HadGEM2-ES_r1_WRF361H	reasonable	good	1.52 (1.1, 1.76)	-0.16 (-0.37, 0.07)	reasonable
IPSL-CM5A-MR_r1_HIRHAM5	good	good	1.42 (1.15, 1.66)	-0.18 (-0.42, 0.03)	good
IPSL-CM5A-MR_r1_RACMO22E	good	good	1.32 (1, 1.59)	0.01 (-0.22, 0.27)	good
IPSL-CM5A-MR_r1_RCA4	reasonable	good	0.86 (0.55, 1.04)	-0.04 (-0.21, 0.41)	reasonable
IPSL-CM5A-MR_r1_REMO2015	good	good	1.51 (1.25, 1.72)	-0.05 (-0.26, 0.13)	good
MIROC5_r1_CCLM4-8-17	good	good	1.94 (1.62, 2.23)	-0.18 (-0.38, -0.04)	reasonable
MIROC5_r1_REMO2015	good	good	2 (1.5, 2.35)	-0.21 (-0.36, 0.03)	reasonable
MPI-ESM-LR_r1_ALADIN63	good	good	1.36 (1.13, 1.56)	-0.17 (-0.34, -0.05)	good
MPI-ESM-LR_r1_CCLM4-8-17	good	good	1.23 (0.98, 1.44)	-0.16 (-0.33, 0.01)	inf_pr
MPI-ESM-LR_r1_COSMO-crCLIM-v1-1	good	good	1.2 (1, 1.35)	-0.18 (-0.39, -0.05)	good
MPI-ESM-LR_r1_HadREM3-GA7-05	good	good	2.82 (1.09, 3.82)	-0.71 (-0.9, -0.02)	inf_pr
MPI-ESM-LR_r1_HIRHAM5	good	good	1.37 (1.15, 1.56)	-0.22 (-0.4, -0.08)	good
MPI-ESM-LR_r1_RACMO22E	good	good	1.38 (1.11, 1.61)	-0.09 (-0.21, 0.06)	good
MPI-ESM-LR_r1_RCA4	good	good	0.82 (0.67, 0.94)	-0.25 (-0.51, -0.1)	bad

MPI-ESM-LR_r1_RegCM4-6	good	good	1.45 (1.08, 1.79)	-0.27 (-0.61, -0.02)	good
MPI-ESM-LR_r1_REMO2009	good	good	1.47 (1.26, 1.68)	-0.26 (-0.48, -0.14)	good
MPI-ESM-LR_r1_WRF361H	reasonable	good	1.31 (1.01, 1.59)	-0.28 (-0.54, -0.1)	reasonable
MPI-ESM-LR_r2_COSMO-crCLIM-v1-1	good	good	1.17 (0.96, 1.37)	-0.04 (-0.18, 0.11)	good
MPI-ESM-LR_r2_RCA4	good	good	1.12 (0.85, 1.34)	-0.17 (-0.47, 0.05)	good
MPI-ESM-LR_r2_REMO2009	good	good	1.53 (1.28, 1.75)	-0.19 (-0.36, -0.04)	good
MPI-ESM-LR_r3_COSMO-crCLIM-v1-1	good	good	1.2 (0.96, 1.38)	-0.12 (-0.27, 0.06)	good
MPI-ESM-LR_r3_RCA4	good	good	1.22 (0.87, 1.54)	-0.28 (-0.58, 0.06)	good
MPI-ESM-LR_r3_REMO2015	good	good	1.64 (1.3, 1.9)	-0.04 (-0.22, 0.14)	good
NorESM1-M_r1_ALADIN63	good	good	1.19 (0.99, 1.41)	-0.07 (-0.38, 0.08)	good
NorESM1-M_r1_COSMO-crCLIM-v1-1	good	good	1.33 (1.05, 1.54)	-0.12 (-0.33, 0.1)	good
NorESM1-M_r1_HadREM3-GA7-05	good	good	2.69 (1.31, 3.59)	-0.63 (-0.9, -0.1)	inf_pr
NorESM1-M_r1_HIRHAM5	good	good	1.56 (1.24, 1.82)	-0.19 (-0.51, -0.03)	good
NorESM1-M_r1_RACMO22E	good	good	1.5 (1.15, 1.78)	-0.18 (-0.36, 0.02)	good
NorESM1-M_r1_RCA4	good	good	1.22 (0.94, 1.46)	-0.22 (-0.6, -0.01)	good
NorESM1-M_r1_RegCM4-6	good	good	1.54 (1.05, 1.87)	-0.2 (-0.49, 0.03)	inf_pr

Table 4.2: *Evaluation of the climate models considered for attribution of Tn14x over Fennoscandia. For each model, the best estimate of the scale and shape parameters is shown, along with a 95% confidence obtained via bootstrapping. The overall evaluation is shown in the right-hand column; only models receiving a category of 'good' overall were included in the final analysis.*

Observations / models	Seasonal	Spatial	Scale parameter	Shape parameter	Overall
ERA5			1.1 (0.82, 1.3)	-0.18 (-0.35, 0.02)	
EOBS			1.04 (0.82, 1.2)	-0.17 (-0.29, 0.01)	
CPC			1 (0.7, 1.21)	-0.25 (-0.51, 0.09)	
ACCESS-CM2_r1	good	good	1.08 (0.84, 1.28)	-0.31 (-0.49, -0.13)	good
ACCESS-ESM1-5_r1	reasonable	reasonable	0.89 (0.69, 1.04)	-0.08 (-0.26, 0.19)	reasonable
AWI-CM-1-1-MR_r1	reasonable	good	1.27 (1, 1.47)	-0.21 (-0.52, 0.01)	reasonable
CMCC-ESM2_r1	reasonable	good	1.06 (0.83, 1.26)	-0.16 (-0.31, 0.04)	reasonable
CNRM-CM6-1_r1	good	good	1.24 (1, 1.45)	-0.29 (-0.49, -0.11)	good
CNRM-CM6-1-HR_r1	good	good	1.09 (0.84, 1.28)	-0.26 (-0.43, -0.07)	inf_pr
EC-Earth3_r1	good	good	1.2 (1, 1.36)	-0.14 (-0.29, 0.02)	good
EC-Earth3-CC_r1	reasonable	good	1.33 (1.02, 1.57)	-0.24 (-0.39, -0.05)	reasonable
EC-Earth3-Veg-LR_r1	reasonable	good	1.11 (0.87, 1.32)	-0.2 (-0.39, 0.05)	reasonable
FGOALS-g3_r1	reasonable	good	1.04 (0.84, 1.2)	-0.22 (-0.4, -0.1)	reasonable
GFDL-CM4_r1	good	good	0.86 (0.68, 1.01)	-0.13 (-0.37, 0.03)	good
GFDL-CM4_r2	good	good	0.87 (0.69, 1.01)	-0.14 (-0.39, 0.02)	duplicate
GFDL-ESM4_r1	reasonable	good	1 (0.82, 1.19)	-0.37 (-0.75, -0.24)	reasonable
HadGEM3-GC31-LL_r1	good	good	1.15 (0.91, 1.34)	-0.33 (-0.47, -0.2)	good
INM-CM4-8_r1	bad	good	0.88 (0.7, 1.01)	-0.14 (-0.4, 0.02)	bad
INM-CM5-0_r1	bad	reasonable	0.69 (0.57, 0.79)	-0.01 (-0.33, 0.17)	bad
IPSL-CM6A-LR_r1	good	good	1.14 (0.95, 1.3)	-0.22 (-0.48, -0.02)	good
KACE-1-0-G_r1	good	good	1.12 (0.94, 1.28)	-0.13 (-0.31, -0.01)	good
KIOST-ESM_r1	bad	bad	0.87 (0.63, 1.04)	-0.28 (-0.49, -0.02)	bad
MPI-ESM1-2-LR_r1	bad	reasonable	0.95 (0.72, 1.11)	-0.15 (-0.29, -0.02)	bad
MRI-ESM2-0_r1	bad	good	1.23 (0.98, 1.59)	-0.21 (-0.71, 0)	bad
NESM3_r1	bad	good	1.5 (1.28, 1.71)	-0.21 (-0.48, -0.04)	bad
NorESM2-LM_r1	bad	reasonable	0.93 (0.75, 1.07)	-0.09 (-0.29, 0.06)	bad
TaiESM1_r1	reasonable	good	0.95 (0.78, 1.1)	-0.17 (-0.33, -0.04)	reasonable
CNRM-CM5_r1_ALADIN63	good	good	1.08 (0.88, 1.24)	-0.17 (-0.39, 0.03)	good
CNRM-CM5_r1_CCLM4-8-17	good	good	1.04 (0.83, 1.27)	-0.19 (-0.49, -0.05)	good
CNRM-CM5_r1_HadREM3-GA7-05	reasonable	good	2.72 (0.71, 3.79)	-0.67 (-0.9, 0.19)	inf_pr
CNRM-CM5_r1_HIRHAM5	good	good	1.03 (0.83, 1.19)	-0.16 (-0.33, 0.02)	good
CNRM-CM5_r1_RACMO22E	good	good	1.04 (0.84, 1.22)	-0.05 (-0.22, 0.13)	good
CNRM-CM5_r1_RCA4	reasonable	good	0.63 (0.46, 0.77)	-0.41 (-0.74, 0.07)	inf_pr
CNRM-CM5_r1_REMO2015	reasonable	good	0.94 (0.78, 1.1)	-0.2 (-0.4, -0.04)	reasonable

EC-EARTH_r12_COSMO-crCLIM-v1-1	good	good	0.93 (0.7, 1.1)	-0.12 (-0.3, 0.15)	duplicate
EC-EARTH_r12_HadREM3-GA7-05	good	good	2.77 (0.75, 3.58)	-0.69 (-0.93, 0.23)	inf_pr
EC-EARTH_r12_HIRHAM5	good	good	1.12 (0.84, 1.35)	-0.22 (-0.45, 0)	duplicate
EC-EARTH_r12_RACMO22E	good	good	1.18 (0.93, 1.4)	-0.19 (-0.43, 0.04)	duplicate
EC-EARTH_r12_RCA4	reasonable	good	0.62 (0.46, 0.76)	-0.29 (-0.65, -0.06)	inf_pr
EC-EARTH_r12_RegCM4-6	good	good	0.71 (0.51, 0.87)	-0.07 (-0.35, 0.23)	good
EC-EARTH_r12_REMO2015	good	good	1.08 (0.85, 1.27)	-0.13 (-0.63, 0.02)	good
EC-EARTH_r12_WRF361H	reasonable	good	0.95 (0.7, 1.13)	-0.16 (-0.35, 0.04)	reasonable
EC-EARTH_r1_COSMO-crCLIM-v1-1	good	good	0.97 (0.77, 1.14)	-0.15 (-0.28, 0)	good
EC-EARTH_r1_HIRHAM5	good	good	1.08 (0.89, 1.24)	-0.21 (-0.37, -0.09)	good
EC-EARTH_r1_RACMO22E	good	good	1.08 (0.9, 1.25)	-0.29 (-0.46, -0.16)	inf_pr
EC-EARTH_r1_RCA4	reasonable	good	0.66 (0.5, 0.77)	-0.16 (-0.46, -0.01)	reasonable
EC-EARTH_r3_COSMO-crCLIM-v1-1	good	good	1 (0.79, 1.15)	-0.15 (-0.37, 0.07)	duplicate
EC-EARTH_r3_HIRHAM5	good	good	0.97 (0.73, 1.17)	-0.07 (-0.32, 0.24)	duplicate
EC-EARTH_r3_RACMO22E	good	good	0.94 (0.74, 1.07)	0 (-0.16, 0.17)	good
EC-EARTH_r3_RCA4	reasonable	good	0.73 (0.56, 0.88)	-0.18 (-0.33, 0.02)	reasonable
HadGEM2-ES_r1_ALADIN63	good	good	1.17 (0.91, 1.35)	-0.25 (-0.49, -0.02)	inf_pr
HadGEM2-ES_r1_CCLM4-8-17	good	good	0.86 (0.69, 1.03)	-0.01 (-0.19, 0.2)	inf_pr
HadGEM2-ES_r1_COSMO-crCLIM-v1-1	good	good	0.97 (0.77, 1.15)	-0.18 (-0.48, 0.06)	good
HadGEM2-ES_r1_HIRHAM5	good	good	1.11 (0.87, 1.35)	-0.25 (-0.54, -0.02)	inf_pr
HadGEM2-ES_r1_RACMO22E	good	good	1.11 (0.91, 1.29)	-0.19 (-0.43, -0.03)	good
HadGEM2-ES_r1_RCA4	good	good	0.79 (0.56, 0.94)	-0.17 (-0.34, 0.13)	good
HadGEM2-ES_r1_RegCM4-6	good	good	0.89 (0.68, 1.05)	-0.17 (-0.38, 0.06)	good
HadGEM2-ES_r1_REMO2015	good	good	0.88 (0.72, 1.08)	-0.37 (-0.67, -0.17)	inf_pr
HadGEM2-ES_r1_WRF361H	good	good	1.05 (0.84, 1.22)	-0.21 (-0.41, -0.01)	good
IPSL-CM5A-MR_r1_HIRHAM5	good	good	0.98 (0.78, 1.17)	-0.08 (-0.29, 0.11)	good
IPSL-CM5A-MR_r1_RACMO22E	good	good	0.84 (0.65, 1.02)	0.06 (-0.14, 0.28)	good
IPSL-CM5A-MR_r1_RCA4	good	good	0.6 (0.43, 0.74)	-0.22 (-0.49, 0.1)	inf_pr
IPSL-CM5A-MR_r1_REMO2015	good	good	0.95 (0.8, 1.09)	-0.2 (-0.4, -0.06)	good
MIROC5_r1_CCLM4-8-17	good	good	1.34 (1.13, 1.55)	-0.13 (-0.36, 0)	reasonable
MIROC5_r1_REMO2015	reasonable	good	1.25 (1, 1.47)	-0.2 (-0.34, -0.02)	reasonable
MPI-ESM-LR_r1_ALADIN63	good	good	0.96 (0.8, 1.08)	-0.2 (-0.36, -0.05)	good
MPI-ESM-LR_r1_CCLM4-8-17	good	good	0.86 (0.7, 1)	-0.21 (-0.36, -0.07)	inf_pr
MPI-ESM-LR_r1_COSMO-crCLIM-v1-1	good	good	0.89 (0.74, 1.03)	-0.33 (-0.47, -0.21)	inf_pr

MPI-ESM-LR_r1_HadREM3-GA7-05	good	good	2.21 (0.75, 2.79)	-0.77 (-0.94, -0.1)	inf_pr
MPI-ESM-LR_r1_HIRHAM5	good	good	0.89 (0.67, 1.05)	-0.2 (-0.39, 0.03)	good
MPI-ESM-LR_r1_RACMO22E	good	good	0.94 (0.72, 1.11)	-0.18 (-0.32, 0.01)	good
MPI-ESM-LR_r1_RCA4	good	good	0.67 (0.49, 0.79)	-0.27 (-0.46, -0.13)	inf_pr
MPI-ESM-LR_r1_RegCM4-6	good	good	0.61 (0.48, 0.73)	-0.35 (-0.63, -0.19)	inf_pr
MPI-ESM-LR_r1_REMO2009	good	good	0.89 (0.72, 1.04)	-0.25 (-0.43, -0.07)	good
MPI-ESM-LR_r1_WRF361H	good	good	0.92 (0.71, 1.14)	-0.44 (-0.8, -0.17)	inf_pr
MPI-ESM-LR_r2_COSMO-crCLIM-v1-1	good	good	0.84 (0.67, 0.99)	-0.09 (-0.22, 0.08)	good
MPI-ESM-LR_r2_RCA4	good	good	0.69 (0.47, 0.83)	-0.1 (-0.27, 0.23)	reasonable
MPI-ESM-LR_r2_REMO2009	good	good	0.94 (0.72, 1.08)	-0.23 (-0.35, -0.08)	good
MPI-ESM-LR_r3_COSMO-crCLIM-v1-1	good	good	0.9 (0.74, 1.04)	-0.22 (-0.39, -0.04)	good
MPI-ESM-LR_r3_RCA4	reasonable	good	0.71 (0.54, 0.87)	-0.37 (-0.7, -0.01)	inf_pr
MPI-ESM-LR_r3_REMO2015	reasonable	good	1.01 (0.8, 1.17)	-0.08 (-0.28, 0.1)	reasonable
NorESM1-M_r1_ALADIN63	good	good	0.91 (0.7, 1.07)	-0.09 (-0.37, 0.07)	good
NorESM1-M_r1_COSMO-crCLIM-v1-1	good	good	0.95 (0.73, 1.13)	0 (-0.18, 0.24)	good
NorESM1-M_r1_HadREM3-GA7-05	good	good	2.14 (0.79, 2.92)	-0.68 (-0.9, 0.09)	inf_pr
NorESM1-M_r1_HIRHAM5	good	good	1.16 (0.96, 1.34)	-0.17 (-0.44, -0.01)	good
NorESM1-M_r1_RACMO22E	good	good	1.03 (0.79, 1.2)	-0.18 (-0.46, 0.03)	good
NorESM1-M_r1_RCA4	good	good	0.67 (0.54, 0.79)	-0.22 (-0.54, -0.05)	inf_pr
NorESM1-M_r1_RegCM4-6	reasonable	good	0.88 (0.67, 1.06)	-0.14 (-0.37, 0.07)	reasonable
NorESM1-M_r1_REMO2015	good	good	0.95 (0.79, 1.09)	-0.09 (-0.26, 0.05)	good

5 Multi-method multi-model attribution

Tables 5.1 and 5.2 show probability ratios (PR) and changes in intensity (ΔI) in each index, for the observational datasets and for those models that passed the evaluation described in section 4. These changes are synthesised into a single overarching attribution result in section 6.

Table 5.1: *(a) Change in intensity and (b) probability ratio intensity for 1-in-50-year Tx14x over the study region, for observational datasets and for each model that passed evaluation: from the 1.3°C cooler preindustrial climate to the present and from the present to 2.6°C above preindustrial (1.3°C warmer than the present). All results are presented to 3 significant figures.*

	(a) Change in intensity		(b) Probability ratio	
Observations / models	**Past - present**	**Present - future**	**Past - present**	**Present - future**
ERA5	2.62 (1.01, 4.21)		Inf (3.86, Inf)	
EOBS	2.02 (0.732, 3.27)		1300 (6.42, Inf)	
CPC	4.4 (1.82, 6.94)		Inf (14.7, Inf)	
ACCESS-CM2_r1	1.79 (0.962, 2.64)	2.09 (1.78, 2.42)	42.9 (4.7, Inf)	7.8 (5.4, 11.9)
CNRM-CM6-1_r1	2.03 (1.33, 2.75)	1.71 (1.49, 1.95)	41.3 (5.33, Inf)	7 (4.81, 12)
EC-Earth3_r1	2.99 (2.23, 3.85)	2.64 (2.29, 3)	16.9 (5.42, 252000)	6.8 (4.64, 11.8)
EC-Earth3-CC_r1	3.32 (2.69, 3.94)	2.68 (2.22, 3.16)	61.6 (10, 15600000)	8.72 (6.28, 12.4)
EC-Earth3-Veg-LR_r1	1.98 (1.05, 2.8)	1.57 (1.11, 2.05)	13.4 (4.05, 1660)	4.84 (3.15, 8.09)
GFDL-CM4_r1	1.99 (1.33, 2.68)	2.07 (1.75, 2.41)	713 (18.3, Inf)	15.6 (10.7, 24.3)
HadGEM3-GC31-LL_r1	2.14 (1.53, 2.81)	2.13 (1.89, 2.38)	256 (11.9, Inf)	10.9 (7.66, 16.7)
IPSL-CM6A-LR_r1	1.88 (1.22, 2.53)	2.03 (1.8, 2.28)	183 (10.9, Inf)	10.7 (8.08, 15)
NESM3_r1	2.02 (1.29, 2.75)	1.72 (1.48, 1.97)	3750 (14.4, Inf)	8.11 (5.96, 12.9)
CanESM2_r1_CCLM4-8-17	1.57 (0.688, 2.38)	1.25 (0.717, 1.89)	4.96 (1.96, 80)	3.46 (1.93, 6.67)
CanESM2_r1_REMO2015	1.36 (0.476, 2.23)	1.32 (0.825, 1.85)	8 (2.04, Inf)	3.98 (2.37, 7.38)
CNRM-CM5_r1_ALADIN63	1.31 (-0.12, 2.81)	1.06 (0.406, 1.72)	67 (0.803, Inf)	5.03 (2.17, 10.4)
CNRM-CM5_r1_CCLM4-8-17	1.55 (0.0727, 3.21)	1.02 (0.444, 1.59)	40 (1.11, Inf)	3.37 (1.88, 5.65)
CNRM-CM5_r1_HIRHAM5	1.89 (0.811, 3.03)	0.809 (0.192, 1.43)	152 (4.3, Inf)	3.69 (1.44, 7.59)
CNRM-CM5_r1_RACMO22E	2.45 (1.2, 3.69)	1.48 (0.802, 2.18)	9.35 (2.39, 15000)	4.04 (2.16, 7.51)
CNRM-CM5_r1_REMO2015	1.98 (0.867, 3.22)	1.25 (0.551, 1.89)	19.9 (2.4, Inf)	4.28 (2.18, 8.53)
EC-EARTH_r12_RegCM4-6	2.18 (0.714, 3.52)	1.89 (1.14, 2.78)	362 (3.47, Inf)	7.12 (2.76, 17.8)
EC-EARTH_r12_REMO2015	0.176 (-1.09, 1.8)	1.08 (0.456, 1.74)	1.2 (0.358, Inf)	2.88 (1.55, 10)
EC-EARTH_r1_COSMO-crCLIM-v1-1	1.4 (0.499, 2.29)	0.997 (0.505, 1.44)	4.18 (1.55, 74)	2.44 (1.59, 4.2)
EC-EARTH_r1_HIRHAM5	1.31 (0.334, 2.4)	1.13 (0.642, 1.62)	31.1 (1.78, Inf)	5.17 (2.77, 9.37)
EC-EARTH_r3_RACMO22E	0.888 (-0.369, 2.21)	1.23 (0.595, 1.86)	4.18 (0.618, Inf)	3.82 (2.02, 7.86)
HadGEM2-ES_r1_ALADIN63	2.76 (1.47, 3.84)	1.96 (1.49, 2.39)	480 (7.45, Inf)	6.69 (3.83, 15.1)
HadGEM2-ES_r1_COSMO-crCLIM-v1-1	1.88 (1.09, 2.7)	1.36 (0.955, 1.77)	132 (5.65, Inf)	5.53 (3.33, 9.5)
HadGEM2-ES_r1_HIRHAM5	2.57 (1.7, 3.46)	1.92 (1.46, 2.41)	195 (5.38, Inf)	9.65 (5.24, 17)
HadGEM2-ES_r1_RACMO22E	2.76 (1.67, 3.78)	1.99 (1.46, 2.49)	85.6 (5.74, Inf)	7.48 (4.68, 12.2)

HadGEM2-ES_r1_RCA4	1.7 (0.516, 2.75)	1.43 (0.942, 1.89)	113 (3.53, Inf)	6.13 (3.31, 13.4)
HadGEM2-ES_r1_RegCM4-6	2.19 (1.08, 3.33)	1.57 (1.07, 2.08)	9.84 (2.66, Inf)	4.77 (2.52, 11)
IPSL-CM5A-MR_r1_HIRHAM5	2.15 (1.19, 3.05)	0.887 (0.362, 1.38)	91.3 (3.35, Inf)	2.93 (1.41, 7.01)
IPSL-CM5A-MR_r1_RACMO22E	2.2 (1.31, 3.02)	0.79 (0.289, 1.31)	4.84 (1.8, 107)	2.11 (1.31, 4.37)
IPSL-CM5A-MR_r1_REMO2015	1.26 (0.294, 2.23)	0.611 (0.136, 1.1)	2.81 (1.27, 32.2)	1.68 (1.13, 3.2)
MPI-ESM-LR_r1_ALADIN63	1.63 (0.749, 2.49)	1.68 (1.02, 2.35)	19.3 (3.16, Inf)	7.15 (3.28, 16.7)
MPI-ESM-LR_r1_COSMO-crCLIM-v1-1	0.747 (-0.0844, 1.56)	0.819 (0.324, 1.34)	4.17 (0.86, Inf)	3.32 (1.58, 7.93)
MPI-ESM-LR_r1_HIRHAM5	0.821 (-0.0986, 1.71)	0.898 (0.283, 1.54)	5.36 (0.828, Inf)	3.81 (1.55, 10.1)
MPI-ESM-LR_r1_RACMO22E	0.788 (-0.141, 1.67)	0.971 (0.126, 1.74)	2.29 (0.878, 10.8)	2.55 (1.1, 5.92)
MPI-ESM-LR_r1_RegCM4-6	0.195 (-1.23, 1.72)	0.733 (-0.0358, 1.51)	1.49 (0.204, Inf)	2.61 (0.933, 7.58)
MPI-ESM-LR_r1_REMO2009	0.596 (-0.299, 1.66)	0.669 (0.0557, 1.4)	3.85 (0.566, Inf)	3.22 (1.12, 12.2)
MPI-ESM-LR_r2_COSMO-crCLIM-v1-1	0.557 (-0.286, 1.5)	0.927 (0.54, 1.36)	1.75 (0.736, 7.45)	2.81 (1.77, 5.25)
MPI-ESM-LR_r2_RCA4	0.382 (-0.843, 1.91)	0.886 (0.462, 1.26)	1.99 (0.389, Inf)	3.64 (1.93, 8.58)
MPI-ESM-LR_r2_REMO2009	0.226 (-0.828, 1.48)	0.789 (0.242, 1.36)	1.37 (0.391, 106)	2.47 (1.37, 4.65)
MPI-ESM-LR_r3_COSMO-crCLIM-v1-1	0.832 (-0.171, 1.88)	0.879 (0.37, 1.47)	3.32 (0.822, 667)	3.53 (1.61, 7.47)
MPI-ESM-LR_r3_RCA4	0.787 (-0.584, 1.97)	0.893 (0.372, 1.56)	17.1 (0.454, Inf)	6.84 (2.47, 13.6)
MPI-ESM-LR_r3_REMO2015	0.739 (-0.394, 2.37)	0.957 (0.395, 1.61)	1.7 (0.776, 10)	2.07 (1.34, 3.94)
NorESM1-M_r1_ALADIN63	2.08 (1.19, 3.03)	2.14 (1.64, 2.65)	12.7 (2.81, Inf)	7.78 (3.82, 21.1)
NorESM1-M_r1_COSMO-crCLIM-v1-1	2.1 (1.17, 3.25)	1.68 (1.18, 2.19)	18.8 (2.73, Inf)	5.79 (2.61, 14.8)
NorESM1-M_r1_HIRHAM5	1.75 (0.65, 2.9)	1.68 (1.01, 2.35)	22.2 (2.3, Inf)	5.71 (2.8, 13.3)
NorESM1-M_r1_RACMO22E	2.08 (1.02, 3.57)	2.1 (1.55, 2.7)	54 (3.07, Inf)	8.85 (4.85, 15.8)
NorESM1-M_r1_RCA4	1.56 (0.249, 2.88)	1.88 (1.2, 2.47)	135 (1.88, Inf)	11.6 (5.4, 26)
NorESM1-M_r1_REMO2015	2.35 (1.03, 3.53)	2.1 (1.51, 2.75)	12.1 (2.45, 1480)	6.07 (3.17, 12.9)

Table 5.2: *(a) Change in intensity and (b) probability ratio intensity for 1-in-20-year Tn14x over the study region, for observational datasets and for each model that passed evaluation: from the 1.3°C cooler preindustrial climate to the present and from the present to 2.6°C above preindustrial (1.3°C warmer than the present). All results are presented to 3 significant figures.*

	(a) Change in intensity (°C)		**(b) Probability ratio**	
Observations / models	**Past - present**	**Present - future**	**Past - present**	**Present - future**
ERA5	2.34 (1.12, 3.51)		538 (4.18, Inf)	
EOBS	1.06 (0.158, 1.84)		7.3 (1.39, 140)	
CPC	2.47 (0.353, 4.26)		Inf (1.49, Inf)	
ACCESS-CM2_r1	1.7 (1.19, 2.25)	1.77 (1.58, 1.95)	927 (22.3, Inf)	8.37 (6.64, 10.6)
CNRM-CM6-1_r1	2.29 (1.72, 2.89)	1.86 (1.69, 2.03)	204 (15.2, Inf)	7.7 (6.17, 9.77)

EC-Earth3_r1	3.01 (2.48, 3.63)	2.62 (2.37, 2.88)	122 (17.4, Inf)	9.78 (7.73, 12.9)
GFDL-CM4_r1	2.29 (1.75, 2.81)	2.01 (1.76, 2.27)	4080 (67.6, Inf)	11.6 (9.33, 14.6)
HadGEM3-GC31-LL_r1	1.99 (1.49, 2.51)	1.86 (1.69, 2.02)	4750 (29.4, Inf)	8.97 (7.42, 11.2)
IPSL-CM6A-LR_r1	1.98 (1.54, 2.48)	2.05 (1.9, 2.24)	144 (14.6, Inf)	10.3 (8.66, 12.5)
KACE-1-0-G_r1	2.68 (2.18, 3.16)	2.42 (2.21, 2.64)	77.6 (16.2, Inf)	9.65 (7.63, 12.5)
CNRM-CM5_r1_ALADIN63	1.81 (0.912, 2.81)	1.39 (0.946, 1.83)	40.2 (4.41, Inf)	5.77 (3.57, 9.15)
CNRM-CM5_r1_CCLM4-8-17	1.65 (0.694, 3.29)	1.16 (0.811, 1.52)	55.3 (2.94, Inf)	4.78 (3.1, 7.68)
CNRM-CM5_r1_HIRHAM5	1.69 (0.824, 2.53)	0.995 (0.543, 1.46)	29 (3.66, Inf)	4.03 (2.32, 6.73)
CNRM-CM5_r1_RACMO22E	2.65 (1.73, 3.56)	1.75 (1.29, 2.21)	22.8 (4.91, Inf)	6.44 (4.01, 10.3)
EC-EARTH_r12_RegCM4-6	2.19 (1.39, 3)	1.81 (1.48, 2.18)	79.3 (4.16, Inf)	10.3 (5.18, 16.3)
EC-EARTH_r12_REMO2015	1.09 (0.107, 1.97)	1.33 (0.91, 1.77)	5.21 (1.18, Inf)	4.59 (2.82, 9.94)
EC-EARTH_r1_COSMO-crCLIM-v1-1	1.38 (0.693, 2.04)	1.24 (0.892, 1.56)	13.8 (3.33, 67600)	5.34 (3.52, 8.54)
EC-EARTH_r1_HIRHAM5	1.14 (0.34, 1.97)	1.16 (0.797, 1.53)	12.2 (1.87, Inf)	4.97 (3.08, 7.76)
EC-EARTH_r3_RACMO22E	1.66 (0.954, 2.4)	1.59 (1.2, 1.99)	5.89 (2.2, 68.1)	4.69 (2.76, 8.72)
HadGEM2-ES_r1_COSMO-crCLIM-v1-1	1.88 (1.33, 2.62)	1.62 (1.35, 1.91)	146 (5.39, Inf)	7.63 (5.3, 10.5)
HadGEM2-ES_r1_RACMO22E	2.51 (1.9, 3.3)	2.09 (1.77, 2.39)	1020 (14, Inf)	9.03 (6.48, 12.7)
HadGEM2-ES_r1_RCA4	1.92 (1.27, 2.62)	1.81 (1.57, 2.08)	840 (6.96, Inf)	12.2 (8.68, 16)
HadGEM2-ES_r1_RegCM4-6	2.04 (1.37, 2.77)	1.7 (1.36, 1.99)	351 (9.17, Inf)	9.38 (6.64, 13.2)
HadGEM2-ES_r1_WRF361H	2.47 (1.63, 3.39)	1.95 (1.57, 2.33)	218000 (14.9, Inf)	10.2 (7.34, 14.4)
IPSL-CM5A-MR_r1_HIRHAM5	2.24 (1.6, 2.9)	1.32 (0.962, 1.65)	28.3 (4.83, Inf)	4.26 (2.78, 6.41)
IPSL-CM5A-MR_r1_RACMO22E	2.58 (1.97, 3.12)	1.55 (1.26, 1.86)	10.3 (3.96, 273)	5.49 (3.79, 8.75)
IPSL-CM5A-MR_r1_REMO2015	1.94 (1.31, 2.66)	1.26 (0.984, 1.56)	730 (11.5, Inf)	5.47 (3.72, 8.44)
MPI-ESM-LR_r1_ALADIN63	1.44 (0.819, 2.04)	1.71 (1.28, 2.18)	48.3 (3.44, Inf)	8.85 (5.32, 13.9)
MPI-ESM-LR_r1_HIRHAM5	1.07 (0.466, 1.66)	1.14 (0.735, 1.53)	17.8 (2.46, Inf)	5.6 (3.08, 10.1)
MPI-ESM-LR_r1_RACMO22E	1.51 (0.941, 2.11)	1.62 (1.16, 2.04)	45.4 (5.32, Inf)	7.31 (4.06, 11.3)
MPI-ESM-LR_r1_REMO2009	1.09 (0.457, 1.67)	1.18 (0.744, 1.6)	61 (2.96, Inf)	6.61 (3.56, 11)
MPI-ESM-LR_r2_COSMO-crCLIM-v1-1	1.1 (0.467, 1.72)	1.19 (0.844, 1.54)	6.35 (1.96, 91.5)	5.16 (3.1, 8.72)
MPI-ESM-LR_r2_REMO2009	0.671 (-0.00837, 1.53)	0.918 (0.555, 1.25)	5.57 (0.988, Inf)	3.72 (2.44, 6.22)
MPI-ESM-LR_r3_COSMO-crCLIM-v1-1	1.24 (0.534, 1.95)	1.15 (0.807, 1.55)	58.8 (3.1, Inf)	6.76 (4.29, 10.3)
NorESM1-M_r1_ALADIN63	2.27 (1.66, 3.02)	2.13 (1.73, 2.5)	45.6 (7.3, Inf)	10.8 (6.81, 16.1)
NorESM1-M_r1_COSMO-crCLIM-v1-1	2.17 (1.52, 3.04)	1.92 (1.49, 2.35)	10.2 (2.68, 1660)	7.64 (4.26, 12.4)
NorESM1-M_r1_HIRHAM5	2.09 (0.96, 3.1)	1.85 (1.36, 2.29)	62.8 (5.49, Inf)	6.9 (4.72, 10.2)
NorESM1-M_r1_RACMO22E	2.42 (1.65, 3.51)	2.25 (1.81, 2.68)	1100 (10.6, Inf)	11.7 (8.4, 15.9)
NorESM1-M_r1_REMO2015	2.49 (1.66, 3.27)	2.03 (1.66, 2.45)	51.2 (8.07, Inf)	9.22 (5.63, 14.5)

6 Hazard synthesis

For both Tx14x and Tn14x, we evaluate the influence of anthropogenic climate change by calculating the probability ratio and change in intensity for similarly extreme events using observation-based products, in this case ERA5 and E-Obs, and climate models. Models which do not pass the evaluation described in section 5 are excluded from the analysis. The aim is to synthesise results from models that pass the evaluation along with the observations-based products, to give an overarching attribution statement. For full details of how the results are synthesised, see Otto et al. (2024).

Figures 6.1 - 6.4 show the synthesised changes in probability and intensity for the observation-based products (blue) and models (red), with the overall synthesised results shown as a purple bar. Because so many climate models passed the evaluation step, these figures only show the synthesised results for the two model ensembles, along with the overarching result. The results are also summarised in Tables 6.1 and 6.2. Plots of attribution results for the individual models can be found in the appendix, in Figures A3.1-A3.8.

6.1 Tx14x

Figure 6.1 shows the synthesised changes in intensity for a 1-in-50-year Tx14x event associated with 1.3°C of warming from the preindustrial period to 2025, and a further 1.3°C of warming from 2025 to the end of the century under current policies. The nine CMIP6 models simulated warming of similar or greater magnitude than the observational data products (Figure A3.1), so that the overall estimated change in intensity is almost identical, but with narrower confidence intervals. Note that the older CMIP5 generation of climate models are known to underestimate temperature trends in northwestern Europe, possibly reflecting missing processes such as feedbacks, changes in circulation patterns or static aerosol forcings (van Oldenborgh et al. 2022; Vautard et al., 2023), whilst this bias is reduced in CMIP6. The thirty-nine CORDEX models, which are driven by the CMIP5 models, typically simulate less warming over the same period than the CMIP6 models (Figure A3.2), although all still simulate a warming trend. The overall synthesis (purple bars) uses a weighted average of all model runs, rather than of all ensembles, and because there are so many more CORDEX runs, they dominate the models' contribution to the overall synthesis, and the overall estimated change in intensity is 2 degrees (estimated 95% interval: 0.4 to 3.5°C). Likewise, the CMIP6 models project a continuation of the observed trend, while the CORDEX models give a lower estimate; the synthesised result from all of the models is a further increase of 1.4°C (estimated 95% interval: 0.4 to 2.5°C) of local warming associated with a further 1.3°C of global warming. However, we stress that due to the sheer number of CORDEX runs in the analysis, this is likely to be a conservative estimate, and it is more likely that the region has warmed by more than two degrees since preindustrial times, with this rate of warming likely to continue.

Figure 6.2 shows the synthesised changes in the likelihood of what is, in 2025, a 1-in-50 year Tx14x event. No estimated PR is given for the observational datasets due to the infinite best estimate produced for ERA5 (Table 3.1), and due to infinite best estimates in six of the nine CMIP6 models and 28 of the 39 CORDEX models, the uncertainties about the estimates are very large. For the 1.3°C of warming already observed, the CMIP6 models - which, as noted above, simulate trends of similar magnitude to the observational datasets - give a best estimate of 46, with a lower bound of 5; for the more conservative CORDEX models the best estimate is about 5, with a lower bound of 0.44. The

synthesised result, taking only the model results into account, is that 14-day heatwaves like the 2025 event are now an estimated 7.4 times more likely than they would have been without human-caused warming. The uncertainty bounds around this number are very wide, largely due to the large proportion of infinite upper bounds estimated from the climate models. This best estimate of 7.4 is consistent with the lower bounds estimated from individual CMIP6 models (Figure A3.3 and Table 5.1), and also with the projected future changes, which are better constrained due to the longer time series used in the model fitting. However, it is important to note that this result does not include any information from the observational time series, due to the infinite estimates in the upper bounds, but that the best estimates of the probability ratio from those datasets were 1300 and infinity; it is therefore clear that the numbers presented here are a very conservative and approximate estimate. We therefore do not report the exact synthesised numbers, but round the best estimate from the models to 'at least ten' times more likely to reflect the order of magnitude of the change, and so to avoid giving a false sense of precision in the results. This result is in line with other recent studies that have found similar or even larger changes in the likelihood of heat extremes in the region (e.g. Leach et al., 2020; Wilcke et al., 2020; Yiou et al., 2020; Rantanen et al. 2024).

	Change in intensity (°C)		**Probability ratio**	
	Already occurred	**Projected**	**Already occurred**	**Projected**
Observations	**2.3 (0.65, 4)**	-	-	-
CMIP6	**2.3 (1.2, 3.3)**	**2.1 (1.3, 2.8)**	**46 (5, 120000)**	**8.7 (4.7, 17)**
CORDEX	**1.5 (0.13, 2.9)**	**1.3 (0.37, 2.2)**	5.3 (0.44, 1100)	**4.2 (1.7, 11)**
Synthesis	**2 (0.42, 3.5)**	**1.4 (0.37, 2.5)**	7.4 (0.39, 3400)	**5.1 (1.8, 15)**

Table 6.1: *Summary of synthesised changes in Tx14x, presented in Figures 6.1 and 6.2. Statistically significant changes are highlighted in* ***bold****.*

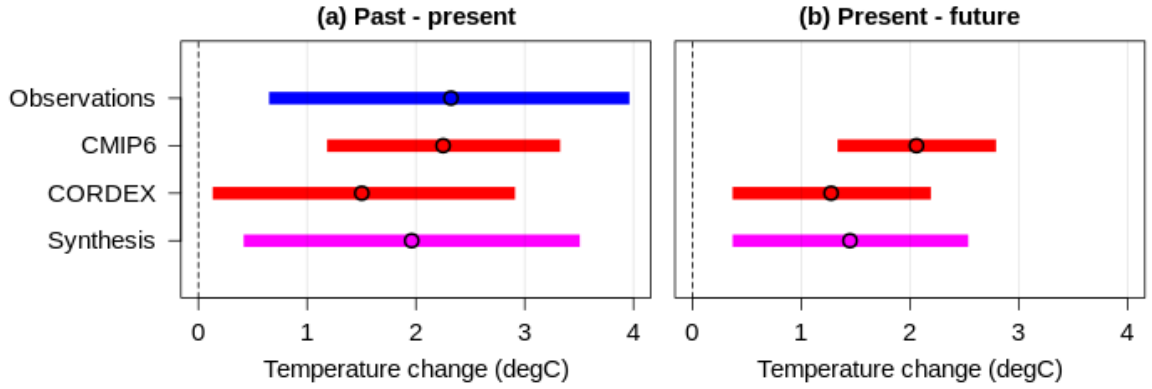

Figure 6.1: *Synthesis of change in intensity of Tx14x in Fennoscandia when comparing (a) the 2025 climate and a 1.3°C cooler climate representing the preindustrial past and (b) the 2025 climate and a 1.3°C warmer climate representing the end of the century under current policies.*

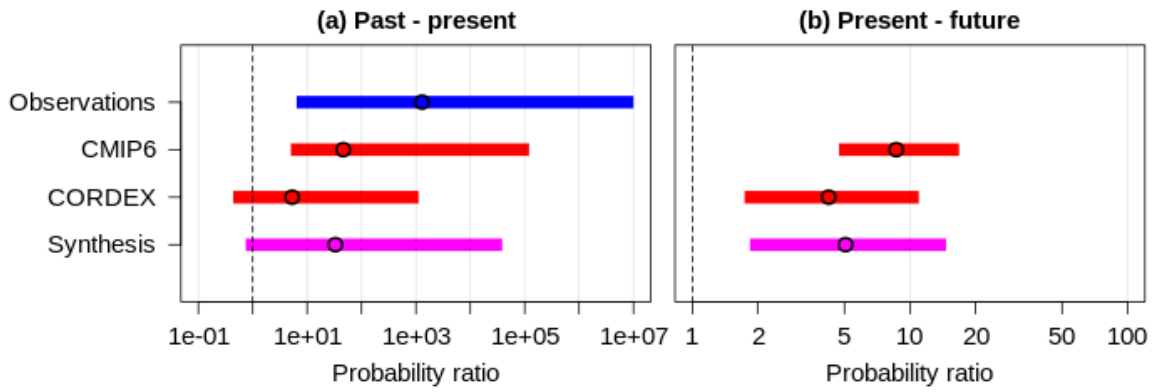

Figure 6.2: *Synthesis of change in likelihood of 1-in-50-year Tx14x in Fennoscandia when comparing (a) the 2025 climate and a 1.3°C cooler climate representing the preindustrial past and (b) the 2025 climate and a 1.3°C warmer climate representing the end of the century under current policies. Note that the x-axes are different.*

6.2 Tn14x

Figure 6.3 shows the synthesised changes in intensity for a 1-in-20-year Tn14x event associated with 1.3°C of warming from the preindustrial period to 2025, and a further 1.3°C of warming from 2025 to the end of the century under current policies. In this case, the seven CMIP6 models simulated warming of similar or greater magnitude than the observational data products (Figure A3.5), while the overall CORDEX models simulate a similar trend. This suggests that the processes leading to the observed warm period prior to 1960, which results in a smaller increasing trend compared to that derived from recent decades alone (see section 3.2), might not be adequately captured in the CMIP6 runs. Taking into account both observations and models, the estimated change in intensity associated with 1.3°C of past warming is 1.9 degrees (estimated 95% interval: 0.48 to 3.2°C), comparable to the estimated warming trend in Tx14x. This warming trend is expected to continue, with a further 1.7°C (estimated 95% interval: 0.84 to 2.5°C) projected if the world reaches 2.6°C above preindustrial temperatures.

Figure 6.4 shows the synthesised changes in the likelihood of what is, in 2025, a 1-in-20 year Tn14x event. In this case we are able to obtain finite estimates for the probability ratio associated with warming that has already occurred, although the uncertainties are again extremely high due to large numbers of models with infinite upper bounds (in ERA5, all of the seven CMIP6 models and 24 of the 29 CORDEX models). The overall synthesis (represented by the purple bars) suggests that similar two-week nighttime heatwaves are around 33 times more likely to occur in 2025 than they would have been in a preindustrial climate, although the uncertainty range about this number is very wide; after a further 1.3°C of warming, similar events are projected to be a further 7.5 times more likely to occur (95% interval: 3.9 to 14 times more likely).

	Change in intensity (°C)		**Probability ratio**	
	Already occurred	**Projected**	**Already occurred**	**Projected**

Observations	1.7 (-0.37, 3.7)	-	63 (0.07, 2500000)	-
CMIP6	**2.3 (1.4, 3.2)**	**2.1 (1.5, 2.7)**	**170 (15, 260000)**	**9.4 (7.3, 12)**
CORDEX	**1.8 (0.72, 2.9)**	**1.5 (0.82, 2.3)**	**18 (2, 6600)**	**6.9 (3.5, 13)**
Synthesis	**1.9 (0.48, 3.2)**	**1.7 (0.84, 2.5)**	33 (0.59, 69000)	**7.5 (3.9, 14)**

Table 6.2: *Summary of synthesised changes in Tn14x, presented in Figures 6.3 and 6.4. Statistically significant changes are highlighted in* ***bold****.*

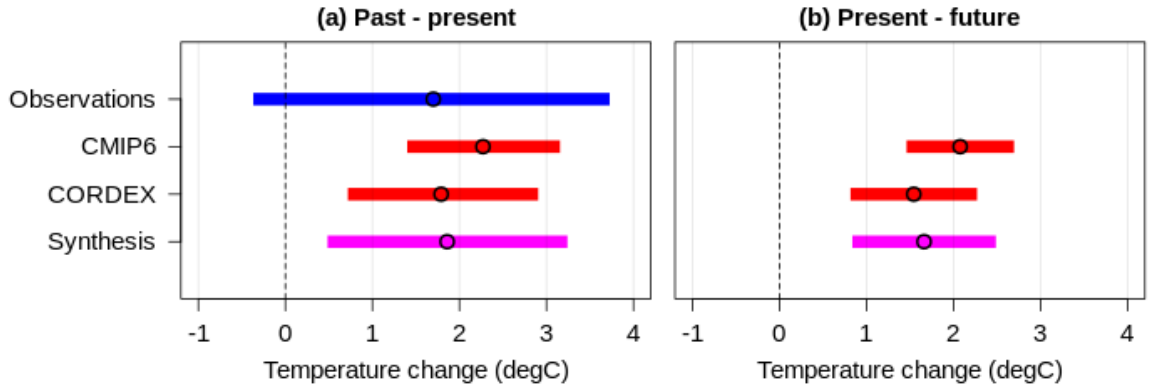

Figure 6.3: *Synthesis of change in intensity of Tn14x in Fennoscandia when comparing (a) the 2025 climate and a 1.3°C cooler climate representing the preindustrial past and (b) the 2025 climate and a 1.3°C warmer climate representing the end of the century under current policies.*

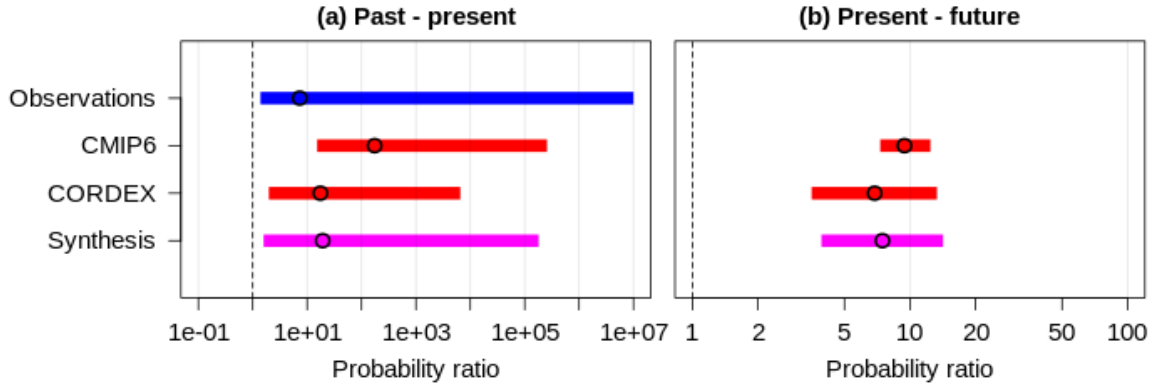

Figure 6.4: *Synthesis of change in likelihood of 1-in-20-year Tn14x in Fennoscandia when comparing (a) the 2025 climate and a 1.3°C cooler climate representing the preindustrial past and (b) the 2025 climate and a 1.3°C warmer climate representing the end of the century under current policies.*

7 Vulnerability and Exposure

The July 2025 heatwave constituted a major climatic event across Fennoscandia, marked by its two-week duration and extensive geographical reach. In both timing and duration, it closely mirrored the 2018 heatwave, though days were slightly hotter (0.6-1C difference) and nights slightly cooler (0.7-1.4C difference) in 2025. Nonetheless, the event brought sustained, impactful heat across urban and rural areas. Unlike 2018's rain-free conditions, intermittent storms and rainfall occurred in July 2025, though they did not sufficiently alleviate localized drought stress.

While it will take weeks to months or even years to uncover the full scope of impacts associated with the 2025 heatwave, the 2018 heatwave remains a critical point of reference for understanding the potential consequences of extended summer heat in the Nordic region. During the 2018 heatwave in Sweden, the combination of extreme heat and dryness was linked to adverse health outcomes, including an estimated 601 to 745 excess deaths, depending on the epidemiological model applied (Åström et al., 2019). At 32% higher than baseline, northern Swedish municipalities such as Umeå, Luleå, and Sundsvall recorded some of the highest relative increases in heat-related mortality nationwide in 2018, suggesting heightened vulnerability in these cooler regions, even though the increase did not reach statistical significance (Åström et al., 2020). It's important to note that mortality is just one indicator, and many people experience health impacts from the heat that are less severe, but nonetheless strain healthcare services. Therefore it's important to also look at other health and care indicators such as increases in ambulance calls or emergency room visits to get a fuller picture of health impacts from heat.

Environmental impacts were also severe in 2018, with widespread water shortages affecting arable land and pastures, leading to a 43% decrease in total harvest compared to the five-year average (Jordbruksverket, 2018) and the worst cereal harvest since the 1950s (SVT, 2018). In Finland, an estimated 380 excess deaths occurred among adults aged over 65 (Finnish Government, 2019), while grain crop yields dropped by about 30% compared to the previous year, particularly in northern regions such as Lapland (Polttimo, 2018). In contrast, Norway found no excess mortality, but the heatwave did significantly impact the agricultural sector, causing a reported 40% decrease in grain production (Knutsen, 2020).

Though cold has historically driven excess mortality in the region, and continues to do so by a substantial margin (García-Leon et al., 2024), heat-related mortality is rising and represents a growing public health concern as climate change increases the intensity, frequency, and duration of heat extremes, while demographic shifts increase the vulnerability (Nordic Health and Welfare Statistics, 2025).

Against this backdrop, it is vital to recognize that Norway, Sweden, and Finland are high-HDI countries, yet this status obscures deep inequities in heat risk. This study focuses on how social dimensions, the built environment, and governance systems shaped the vulnerability, exposure, impacts, and responses associated with the 2025 event.

7.1 Social Dimensions of Heat Risk

7.1.1 Care and social services

The July 2025 heatwave coincided with the peak Nordic summer holiday period, resulting in notable reductions in staffing across healthcare, social services, and municipal functions in Norway, Sweden, and Finland. In a report ahead of the summer, the Swedish National Board of Health and Welfare (*Socialstyrelsen*) (2025) concluded that staffing shortages were again a concern with a majority of Swedish municipalities reporting insufficient summer substitutes in elderly care facilities. While most described the gaps as small, one in five assessed them as fairly large or very large, and shortages were especially acute in parts of northern Sweden, where structural labour constraints, competition from other sectors, and long distances, compounded recruitment challenges - and likewise where the heat was most pronounced during the heatwave. In some municipalities, social activities and lower-priority services were expected to be reduced, and medication management placed extra strain on remaining staff due to fewer trained personnel (Socialstyrelsen, 2025). Furthermore, social and healthcare workers don't always recognise heat as a significant health risk factor, even though they are critical resources for protecting at-risk grounds in care facilities and nursing homes (WHO, 2021).

These limitations extended beyond formal service delivery, as seasonal declines in voluntary engagement, including from organizations such as the Red Cross, further constrained response capacity. Informal social support networks were likewise weakened, with many residents away on holiday, reducing the viability of everyday check-ins and mutual aid among various social connections. This convergence of gaps in formal, voluntary, and informal support structures exposes a layered fragility in care during periods of heightened risk - especially in contexts such as Sweden, where more than 33% of the population over 60 years live alone (Statistics Sweden, 2022).

Institutional care and education services - such as elderly care facilities, homecare, kindergartens, and schools - represent critical points of vulnerability during heatwaves. For example, in Norway, at least 8 hospitals across the country have reported high indoor temperatures which have disrupted care, including cancelled surgeries (TV2, 2025). These settings often serve populations that are physiologically sensitive to heat, including older adults, preschool-aged children, and individuals with chronic conditions. In elderly care facilities across Norway, Sweden, and Finland, risks are amplified by aging populations and infrastructural limitations; many buildings lack adequate cooling, and residents, particularly those with cardiovascular disease, dementia, or respiratory illness, face heightened risk of hospitalization or death during extreme heat events (Astone et al., 2022; Fernandez et al., 2025; Ruuhela et al., 2020; Kollanus et al., 2021; Åström et al., 2020). Similarly, preschools and kindergartens often struggle with high indoor and outdoor temperatures, especially where shaded play areas are insufficient. In Sweden, young children typically spend several hours outdoors daily, and heat stress has been shown to reduce physical activity and increase discomfort in poorly designed yards (Wallenberg et al., 2023; Pagels et al., 2013; Ylvisåker et al., 2021). The 2018 heatwave in Sweden exposed many of these systemic weaknesses. Elderly care units and homecare services struggled to maintain routines due to understaffing and reliance on inexperienced substitutes (Håkansson et al., 2023; Rousi et al., 2023). Staff often improvised coping strategies with limited institutional guidance, while care workers experienced "double exposure" - managing personal heat stress while attending to others (Håkansson et al., 2023). Educators were similarly affected, with dangerously high indoor temperatures and a lack of coordinated response. This exemplifies that heat

is not only an issue for service users, but also an occupational health and safety issue for workers, especially those with physically demanding jobs in buildings with poor ventilation and no active cooling.

7.1.2 Demographics

Housing in Finland, Sweden, and Norway has traditionally been optimized for cold climates, with lack of shading and limited ventilation, making buildings prone to overheating during summer heatwaves. This presents rising health risks, particularly for elderly residents who are more physiologically sensitive to heat and tend to spend more time indoors, especially in care homes or limited-mobility settings (Rousi et al., 2023; Kollanus, Tiittanen & Lanki, 2021). Demographic changes amplify these risks: the populations in the countries are aging rapidly, with those aged over 65 now comprising 18.8% in Norway (Trading Economics, 2025a), 20.6% in Sweden (Trading Economics, 2025b), and over 22% in Finland (Trading Economics, 2025c) - the fastest-aging of the three. This trend, driven by low fertility and rising life expectancy (Heleniak, 2023), amplifies the need for housing and healthcare systems to plan for heat risk. Finland's sustained natural population decline and Sweden's growing 80+ cohort further strain elderly care. By 2040, one in four Nordic residents will be over 65, while the share of young people continues to shrink (The Nordic Council and the Nordic Council of Ministers, n.d.), reinforcing the urgency of age-sensitive adaptation across built environments and care systems.

More frequent exposure to heat also disproportionately affects socioeconomically disadvantaged groups, who tend to live in lower-quality housing with less capacity for adequate ventilation or cooling. In Sweden's *miljonprogramområden*, for example, large households often occupy compact, poorly ventilated apartments during heatwaves (Georgelis & Eriksson, 2017; Formas, n.d.). A nationwide Swedish study found that heatwaves significantly increased all-cause and coronary heart disease (CHD) mortality, but also revealed important socioeconomic disparities (Åström et al., 2020). While neighborhood deprivation did not modify all-cause mortality, it significantly increased CHD mortality during moderate heatwaves, with residents in the most deprived areas facing up to 29% higher risk compared to those in affluent neighborhoods. Similarly, in the first nationwide assessment of temperature-related mortality in Norway, Fernández et al. (2025) found that socioeconomic vulnerability - measured through education, income, urbanization, and access to healthcare - was a key modifier. Municipalities with lower tertiary education levels, lower incomes, and longer driving times to hospitals faced significantly higher mortality from heat. Interestingly, heat-related mortality was higher in medium- and sparsely populated areas, contrary to typical urban-focused assumptions. In Finland, Päivärinne et al. (2025) found that individuals with low socioeconomic status have significantly higher heat vulnerability, even after adjusting for gender and age, with a slightly stronger association among men and those aged over 65. Together, these findings highlight how structural inequality intersects with environmental exposure, producing uneven heat-related health outcomes even in high-income, temperate settings.

7.1.3 Outdoor workers

Due to intensifying, more frequent, and prolonged heat events, outdoor workers are likewise facing increasing exposure to heat. Sectors with labor-intensive outdoor work (e.g. construction, agriculture,

forestry, and municipal services) are especially affected. Road maintenance and construction work is particularly concentrated in the summer months across Sweden, Norway, and Finland, when weather conditions are most favourable. This seasonal pattern, combined with aging infrastructure and growing traffic volumes, has led to an overall increase in the number and scale of such infrastructure improvement projects (Trafikverket, 2022) - intensifying occupational heat exposure during the hottest period of the year. However, protective regulations for these industries are quite strong in Nordic countries due to strong trade unions (Hanvold et al., 2019).

7.1.4 Cultural practices

Longstanding Nordic summer traditions, such as spending extended periods in non-insulated summer cabins, camping, and increased alcohol consumption, may unintentionally heighten vulnerability during periods of extreme heat. These practices often involve limited access to active cooling, high physical exertion, and dehydration risks, particularly in remote or lightly serviced areas. When temperatures are high, more people often go swimming and there has been a notable uptick in drownings in July 2025 in Sweden (31) and Finland (28) (Svenskalivraddningssallskapet, 2025; Suomen Uimaopetus, 2025). In Sweden swimming skills are trending down amongst children and tend to be lower for immigrants than for the general population (Hejdelind, 2025). The Swedish Tourist Association (STF) shared observations with the authors indicating increased tent hiking during warm periods, which may exacerbate thermal discomfort by trapping heat, along with emerging challenges related to water access and hygiene in mountain areas. Drying streams complicated water resupply during a time of increased hydration needs, and the risk of gastrointestinal illness rose linked to increased shared use of natural water sources among humans and animals. At the same time, increased tourism in the post-Covid period has placed additional strain on local healthcare services, emergency response capacity, and water infrastructure (Myndigheten för tillväxtpolitiska utvärderingar och analyser, 2021; Hansen, Arce & Lindberg, 2021), especially in regions already facing structural heat-related vulnerabilities.

7.1.5 Indigenous livelihoods

The July heatwave also underscored how climate extremes intersect with Indigenous livelihoods. The Sámi are the Indigenous people of northern Fennoscandia, with traditional territories across Norway, Sweden, Finland, and the Kola Peninsula in Russia - a region called Sápmi. Reindeer herding is a central aspect of Sámi culture, economy, and identity, with deep ties to land, seasonal cycles, and traditional ecological knowledge passed down across generations. During the 2025 heatwave, reindeer across Finland were reported to move into cities and villages in search of relief from the heat (Mesa, 2025; Benke, 2025), where reindeer fatalities have been reported. Similarly, in Sweden, reindeer were observed seeking shade in lower-altitude villages around Deärnná/Tärnaby and migrating westward from Gávtjávrrie/Ammarnäs toward Norway (SVT, 2025). These disruptions to reindeer migration and grazing illustrate the growing strain that climate extremes place on Sámi livelihoods and traditional practices. In response to such compounding pressures, Sámi communities across the region have increasingly mobilized to strengthen climate resilience on their own terms. In Finland, the Sámi Climate Council, established in 2023, brings together traditional Sámi knowledge holders and scientists to assess the impacts of national climate policy and support culturally grounded adaptation

strategies. In Sweden, a collaborative initiative involving the Sámi Parliament, county administrators, the National Union of the Swedish Sámi People (SSR), and the Swedish Meteorological and Hydrological Institute (SMHI) supports Sámi villages in carrying out detailed climate risk and vulnerability assessments (SMHI, 2025). Led by the Sámi villages themselves, the work combines local ecological knowledge with scientific methods to address challenges. Gran Sámi village, for example, has begun adjusting pasture use and reindeer management in response to these assessments (SMHI, 2025; Gran sameby, n.d.). An external evaluation by WSP (2023), commissioned by the County Administrative Boards, found that the climate and vulnerability assessments carried out by the Sámi villages strengthened internal dialogue, raised awareness of climate risks - especially for reindeer grazing - and effectively integrated traditional and scientific knowledge. The Sámi-led process was key to its legitimacy and impact, laying a strong foundation for long-term, community-driven adaptation - an approach that aligns with broader Sámi calls to frame climate change, including extreme heat, as a human rights issue requiring culturally appropriate adaptation efforts rooted in Indigenous rights and traditional knowledge.

These social vulnerabilities are deeply intertwined with the physical characteristics of the built environment, where outdated infrastructure and poor heat adaptation further compound exposure.

7.2 Infrastructure and Built Environment

Urbanization across Finland, Sweden, and Norway remains high and steadily increasing, with 86, 89, and 84% of the population, respectively, now living in urban areas (World Bank, 2024a; 2024b; 2024c). Recent urban population growth rates range from approximately 0.6% in Sweden to 1.3% in Norway (World Bank, 2024d; 2024e; 2025f), reflecting modest but sustained expansion.

Despite high urbanization rates, coverage and access to green (vegetation-based) and blue (water-based) spaces remains relatively high across Nordic cities. These natural infrastructures are increasingly recognized for their contributions to climate adaptation, physical and mental health, and urban liveability (NORDGREEN, 2024). In cities such as Espoo and Ii (Finland), Täby and Vilhelmina (Sweden), and Stavanger (Norway), over 90% of residents live within 300 meters of a green space. Espoo stands out with 43.5% of its area covered by parks and forests. Despite this, a study by Taylor et al. (2025) investigating the urban heat island (UHI) effect in cold-climate urban areas found that the city of Espoo experiences up to 9°C higher temperatures compared to rural surroundings. In Helsinki, the maximum temperature difference was even higher, of about 14°C. In Sweden, Stockholm, Malmö and Göteborg exhibit measurable UHI effects by up to 7°C compared between highly densely built-up and populated Stockholm and less-so Linköping and Norrköping (Wang et al., 2025). In Norway, areas with trees had temperatures up to 10°C cooler than built up areas (Venter et al., 2020).

While access to natural infrastructures is generally strong, and blue spaces, prominent across the countries, offer additional cooling, planning efforts increasingly focus on addressing inequities in disadvantaged neighborhoods. For example, in lower-income or high-density areas, where vegetation tends to be lower and vulnerability to heat stress higher. In Stavanger, Norway, city planners apply the “3-30-300 rule:” every resident should live within 300 meters of green space, have at least 30% tree canopy cover in streets, and no residence more than a 3-minute walk from a park - promoting

equitable heat mitigation (Lempa & Knudsen, n.d.; Huynh, Salolammi & Borges, 2022). Täby, a municipality in Greater Stockholm, has a newly adopted "green plan" plans for half the municipality to be green, emphasizing equitable distribution of green corridors and recreational spaces (NORDGREEN, 2024). The Swedish Environmental Protection Agency (Naturvårdsverket) and Swedish National Board of Housing, Building and Planning (Boverket) also provide guidance on how to include green areas in urban planning (Naturvårdsverket, 2025).

Due to dense development and UHI effects, urban areas face heightened indoor temperature risks, yet regulatory and adaptation responses remain uneven across the Nordic countries. Finland and Sweden plan to introduce mandatory climate impact assessments for new construction by 2025, with Sweden extending these to renovations by 2027. Norway, by contrast, currently lacks binding requirements for renovation-related adaptation. More broadly, renovation efforts tend to reflect socioeconomic disparities, with wealthier households better able to invest in upgrades such as insulation, shading, or cooling systems. Renters may face additional hurdles, needing permission from landlords to make alternations (infofinland, 2025). Despite ongoing policy progress, much of the existing housing stock continues to reflect historical inequalities in building quality (Balouktsi et al., n.d.). A study by Farahani et al. (2024) evaluating the thermal resilience of Finnish residential buildings under hot summers show that lightweight detached houses respond fastest to outdoor heat, while newer code-compliant buildings have lower indoor temperatures but still exceed health thresholds. Passive measures like ventilation and solar-protective glazing reduce overheating but are insufficient alone, active cooling is necessary, with modest energy demand relative to heating (Farahani et al., 2024).

Access to active cooling in Nordic households remains relatively limited compared to warmer regions, but is increasing due to the widespread adoption of heat pumps - with approximately 60 units per 100 households in Norway, 52.4 per 100 in Finland, and 40 per 100 in Sweden (EHPA, n.d.). These systems, unlike traditional air conditioning (AC) units, serve dual heating and cooling functions, and now constitute the primary form of mechanical cooling across the region. However, the 2018 heatwave revealed how Nordic buildings - including both private homes, care facilities and preschools - designed for winter insulation became dangerously hot during summer. Many lacked active cooling, and even new preschools often lacked shading from trees or structures (Håkansson et al., 2023). HVAC technicians reported limited capacity to mitigate indoor temperatures, particularly in heat-prone UHI areas. Short-term fixes like portable fans and AC units were inconsistently used and constrained by policy, which discouraged permanent cooling systems (Håkansson et al., 2023). A study by Hyyrynen et al. (2025) evaluates the economic feasibility of adapting to rising heat-related mortality in southern Finland through enhanced residential cooling. Using Monte Carlo simulations, the study estimates a tenfold increase in mortality due to heatwaves and demonstrates that while cooling interventions are costly (38,200-416,000€ per life saved), their benefits exceed costs by 1.8 to 18 times under various climate scenarios.

While the heatwave had the potential to strain critical infrastructures across the Nordic countries, no major service breakdowns were reported. Some rail services operated at reduced capacity due to heat-related safety constraints, underscoring rail as a persistent vulnerability during prolonged warm periods. Nordic infrastructure systems incorporate a range of measures to manage climate risks, including renewable energy integration and cross-sector coordination. Norway's transport strategy prioritizes hazard-ready infrastructure, while Sweden's extensive district heating and cooling systems ensure priority supply for hospitals and critical facilities.

The effectiveness of these physical systems is closely tied to governance arrangements that determine how risks are monitored, responsibilities allocated, and resources mobilized during climate shocks like extreme heat.

7.3 Ecological risks

Heatwaves in Finland, Norway and Sweden impact the natural environment including aquatic and terrestrial ecosystems. For example, one study found tree cover loss across northern Europe as a result of heat and drought events from 2018 - 2020 (Knutzen et al., 2025). Extreme heat can amplify conditions like nutrient availability in water bodies, leading to large algal blooms (Szydlowski et al., 2025). Algal blooms can degrade water quality, lead to "dead zones" with low or no oxygen, and release harmful toxins that affect lake ecosystems, drinking water, and recreation (Rutgersson, et al., 2022; EPA, 2025). In the Gulf of Finland in 2018, the warm summer led to exceptional cyanobacterial blooms, leading to the closure of bathing sites (Rutgersson, et al., 2022). Other impacts can include the thawing of permafrost, which constitutes a negative feedback loop as methane, a potent greenhouse gas, is released into the atmosphere (Rößger, N., 2022). Terrestrial species are also moving northward, altering the species living in the boreal and alpine tundra and leading to an increase in shrubs in the high arctic tundra (Bednar-Friedl, B. et al., 2022) There has also been an observed shift in the ranges and compositions of coastal and marine species in northern Europe (Bednar-Friedl, B. et al., 2022). However, there is a need for more research on the specific observed changes to ecosystems in Fennoscandia as a result of extreme heat and many societally relevant research questions remain unanswered (Kebir et al., 2023).

7.4 Heat Risk Governance

Effective governance is a key determinant of heat resilience, shaping how well countries prepare for and respond to extreme heat events. In Nordic countries like Finland, Sweden, and Norway, governance frameworks emphasize shared responsibility, cross-sector coordination, legal mandates, and localized implementation. In recent decades, and following the 2018 heatwave in particular, which exposed significant gaps in preparedness and coordination, all three countries have taken steps to improve risk assessments, strengthen institutional responsibilities, and embed adaptation more deeply into climate and public health policy.

For example, in Norway, the heatwave highlighted the need for clearer institutional responsibilities and catalyzed efforts to embed heat adaptation more systematically within existing climate frameworks. Under the Climate Change Act (2017), all ministries are now mandated to integrate adaptation into their sectoral policies, with coordination led by the Ministry of Climate and Environment (2025). However, there are challenges to translate policies into practice, such as lack of a national heat risk assessment, and only 14 out of 174 municipalities participating in a survey, having indicated that they implemented measures against heatwaves by 2023 (CICERO, 2023).

On city level, Oslo has developed a city-wide adaptation strategy that explicitly addresses rising heat risks. Key measures include mapping urban heat islands, prioritizing green infrastructure like tree planting and park access, and incorporating heat resilience into building and spatial planning

regulations. The city also emphasizes equity by targeting vulnerable populations in its planning and has piloted adaptation measures in specific districts such as Grünerløkka. Heat risk is now more explicitly integrated into Norway's broader climate adaptation strategy (Ministry of Climate and Environment, 2025).

In Finland, heat-health risks are systematically integrated within its broader climate and public health governance frameworks. The National Climate Change Adaptation Plan 2030 addressed heatwaves as part of multisectoral climate risk management, including targets for health and social services preparedness (Finnish Government, 2024). Municipalities are expected to incorporate heat-health risks into welfare and safety planning, including preparedness in elderly care and social services (Hyyrynen et al., 2025). For example, Helsinki's Climate Adaptation Strategy (2019-2025) prioritizes comprehensive risk mapping, identifying vulnerable populations and infrastructure, including healthcare facilities (City of Helsinki, 2019). According to a 2022 survey of 141 respondents from hospitals across Finland, just over half of the facilities assessed problems with indoor overheating, and based on this many facilities planned to take heat-related disruptions into account in their preparedness plans (Kollanus et al., 2022). Adaptation is also integrated into land-use planning, public building management, and greening efforts such as green roofs and district cooling to mitigate UHI effects (Sweco Group, 2024).

In Sweden, the 2018 heatwave revealed systemic shortcomings in heat preparedness and response, including unclear institutional responsibilities, limited understanding of compounding (heat + drought) climate risks, limited local coordination, and inadequate integration of climate risks into social and health services, underscoring the need for more coherent and proactive heat risk governance across sectors (Rousi et al., 2023). Sweden's national Climate Policy Council has called for stronger cross-sectoral collaboration after 2018, but follow-up at the municipal level has been uneven, particularly in settings where staffing, funding, and institutional continuity is limited (Klimatanpassningsrådet, 2022; SOU 2025:51). Since 2018, national agencies including the Swedish National Board of Health and Welfare (*Socialstyrelsen*), Swedish Civil Contingencies Agency (*Myndigheten för samhällsskydd och beredskap (MSB)*), and Public Health Agency (*Folkhälsomyndigheten*) have developed a clearer framework for heatwave preparedness, with guidance, oversight, and targeted support for municipalities, regions, and care providers - especially those serving high-risk groups such as older adults, chronically ill individuals, and persons with disabilities (Kunskapsguiden, n.d.; Vårdgivarguiden, n.d.; Folkhälsomyndigheten, n.d.; MSB, n.d.). However, the translation of these high-level plans into consistent, actionable routines remains a challenge. Few care organizations conducted formal evaluations or implemented structural changes (Håkansson et al., 2023). While "mental preparedness" among managers has improved, fragmented responsibilities between municipal and private actors still hinder coordinated adaptation. Nevertheless, emerging practices such as the use of a "year wheel" to structure seasonal preparedness - used by one home for the elderly to pre-schedule actions like requesting summer clothing from relatives, checking blinds, and preparing hydration routines (Håkansson et al., 2023) - may offer scalable models for long-term heat resilience. It's too early to know whether the implementation of such preparedness efforts may already be helping to reduce immediate health impacts compared with 2018.

V&E Conclusions

The 2025 heatwave illustrates how heat risk in Sweden, Finland, and Norway is driven by the intersection of demographic change, built environment vulnerabilities, and uneven adaptive capacity. An aging population - already among the oldest in Europe - faces heightened physiological susceptibility to heat, particularly in care facilities and private homes designed for cold climates, where building design and limited ventilation exacerbate overheating. Seasonal staffing shortages in health and social care and reduced informal support during the holiday period, and persistent gaps in risk awareness, further undermine resilience. Socioeconomic inequities deepen these vulnerabilities, as low-income and socio-spatially deprived communities are more likely to occupy poorly adapted housing in heat-prone urban heat islands, with restricted access to active cooling. Outdoor workers, certain tourism practices, and Indigenous Sámi livelihoods also emerge as distinct exposure pathways, underscoring the diverse social dimensions of heat risk across Finland, Sweden, and Norway.

Yet, recent years have brought measurable progress in adaptation governance, preparedness and urban planning. Since 2018, all three countries have advanced heat action planning, integrated equity considerations into greening strategies, and expanded the use of nature-based solutions to mitigate urban heat. Municipal innovations - from Stavanger's 3-30-300 green infrastructure rule to Helsinki's integration of heat risk into land-use and building regulation - signal a shift toward systemic, place-based adaptation. In Sweden, national agencies have developed clearer heatwave preparedness frameworks for municipalities, regions, and care providers, with targeted guidance for elderly care, homecare services, and other high-risk settings. The persistence of intersecting, structural inequities in housing quality, gaps in care system preparedness, and the accelerating pace of demographic aging indicate that without deeper structural adaptation, heat risk will continue to exacerbate as climate extremes intensify.

Data availability

All time series used in the attribution analysis are available via the Climate Explorer.

References

All references are given as hyperlinks in the text.

Appendix

A.1 Additional figures

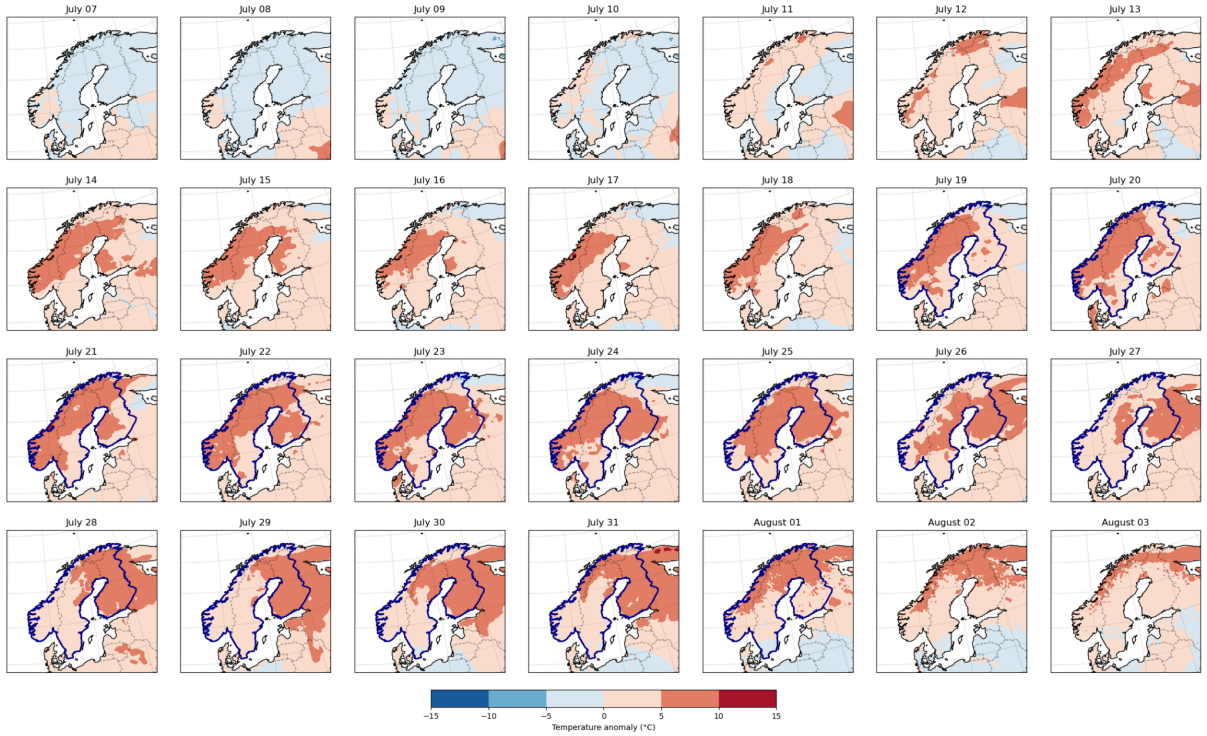

Figure A1.1: *Daily minimum temperature anomalies with respect to the 1990-2020 July climatology (ERA5). The study region is outlined in dark blue during the event period (hottest 14-day period averaged over the entire region).*

A.2 Model evaluation plots

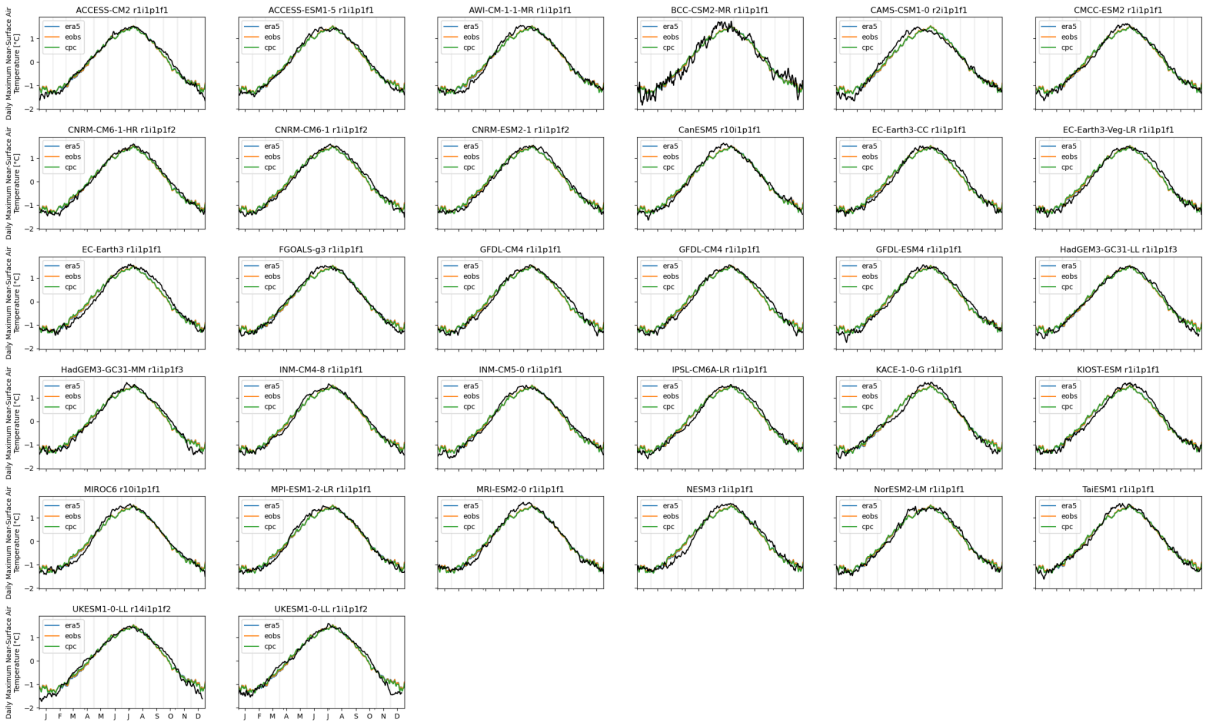

Figure A2.1: *Plots of seasonal cycle of daily maximum temperatures over Fennoscandia in CMIP6 models, scaled to have mean 0 and standard deviation 1.*

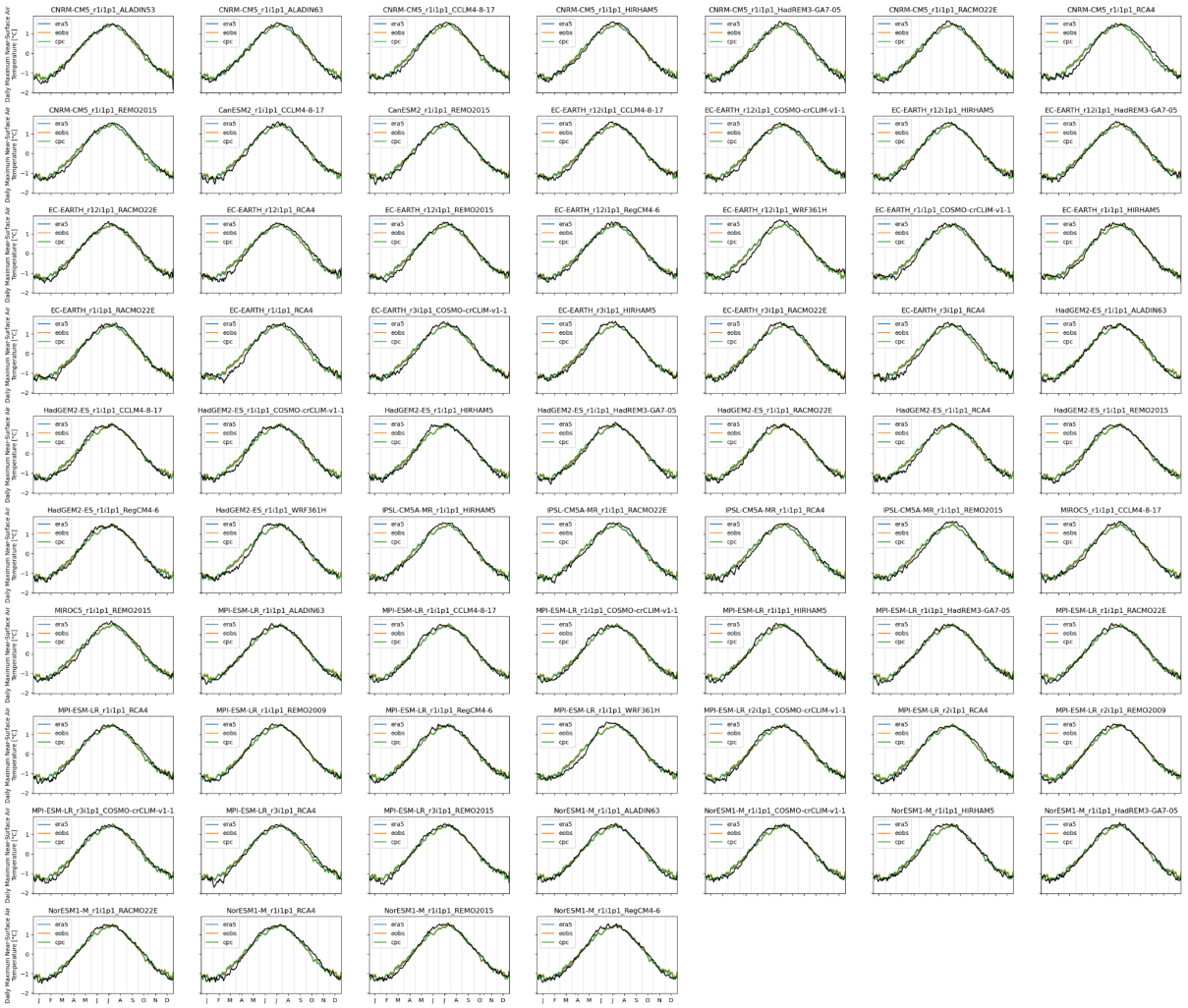

Figure A2.2: *Plots of seasonal cycle of daily maximum temperatures over Fennoscandia in CORDEX models, scaled to have mean 0 and standard deviation 1.*

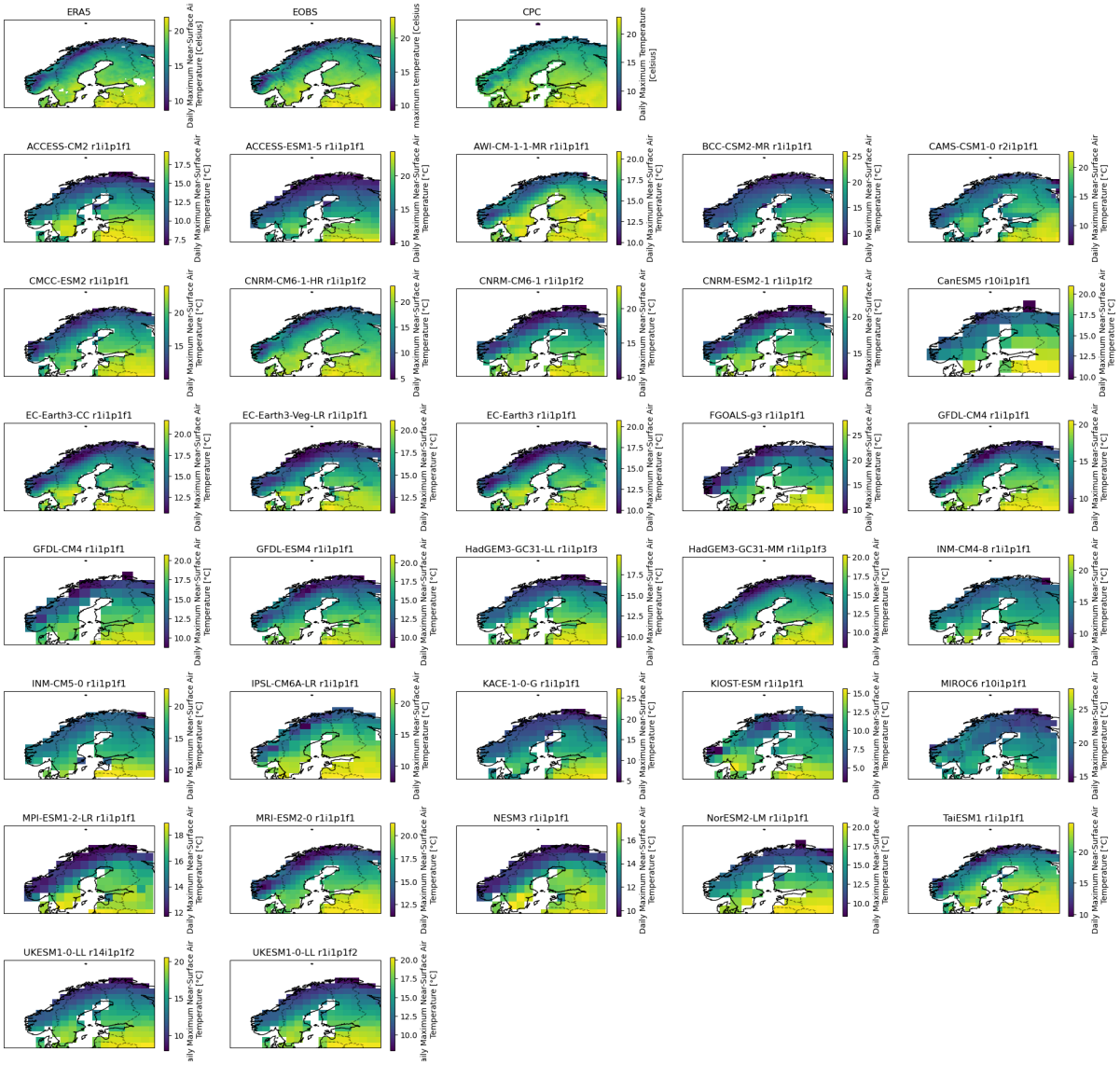

Figure A2.3: *Plots of spatial pattern of June-August mean of daily maximum temperatures over Fennoscandia in CMIP6 models and observational datasets.*

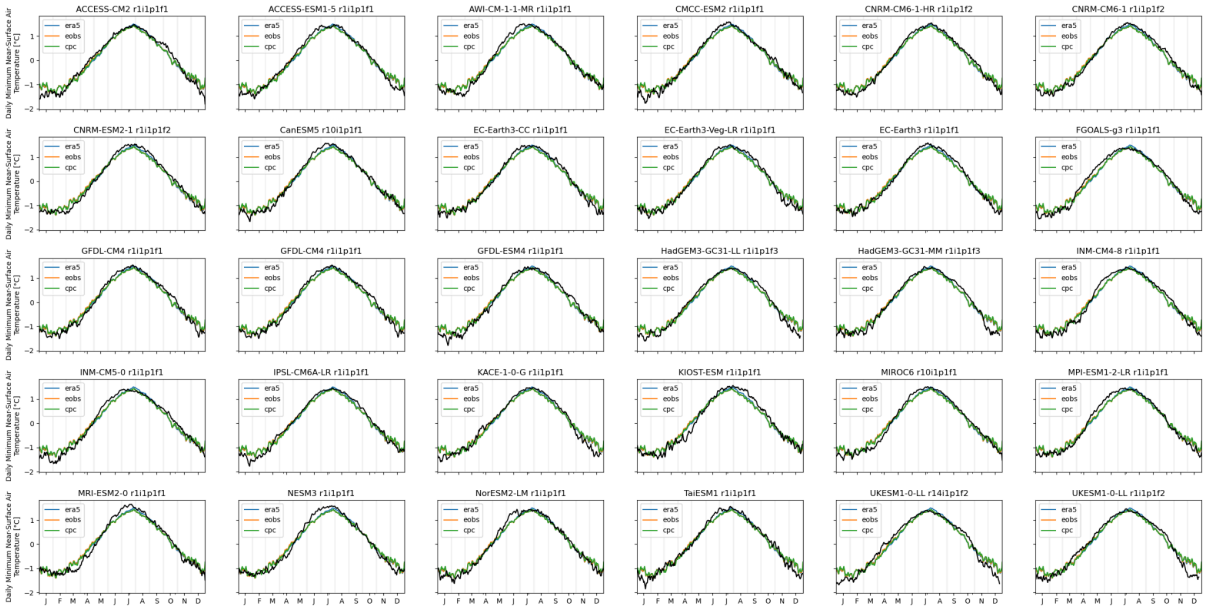

Figure A2.4: *Plots of seasonal cycle of daily minimum temperatures over Fennoscandia in CMIP6 models, scaled to have mean 0 and standard deviation 1.*

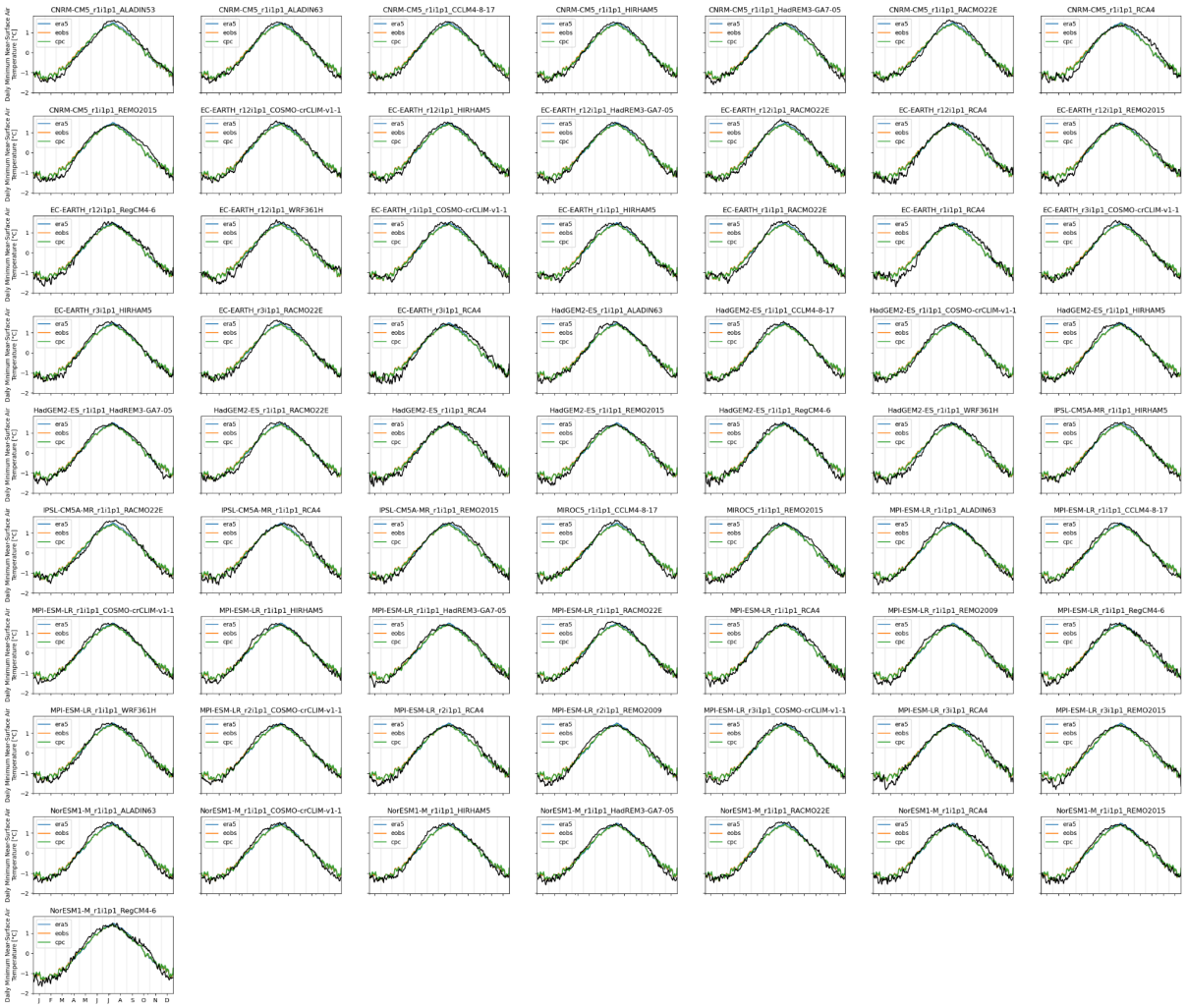

Figure A2.5: *Plots of seasonal cycle of daily minimum temperatures over Fennoscandia in CORDEX models, scaled to have mean 0 and standard deviation 1.*

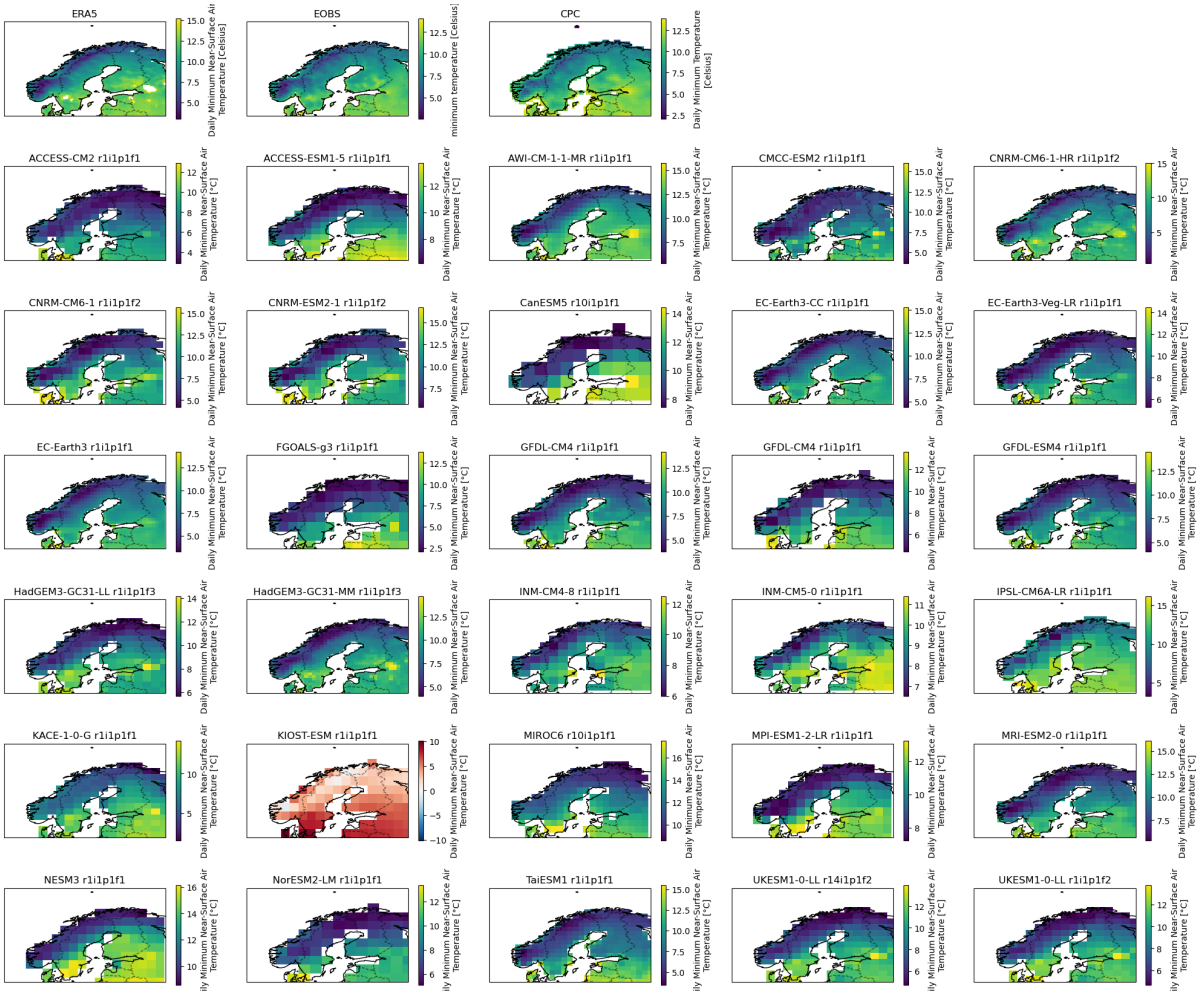

Figure A2.6: *Plots of spatial pattern of June-August mean of daily minimum temperatures over Fennoscandia in CMIP6 models and observational datasets.*

A.3 Attribution plots for individual climate models

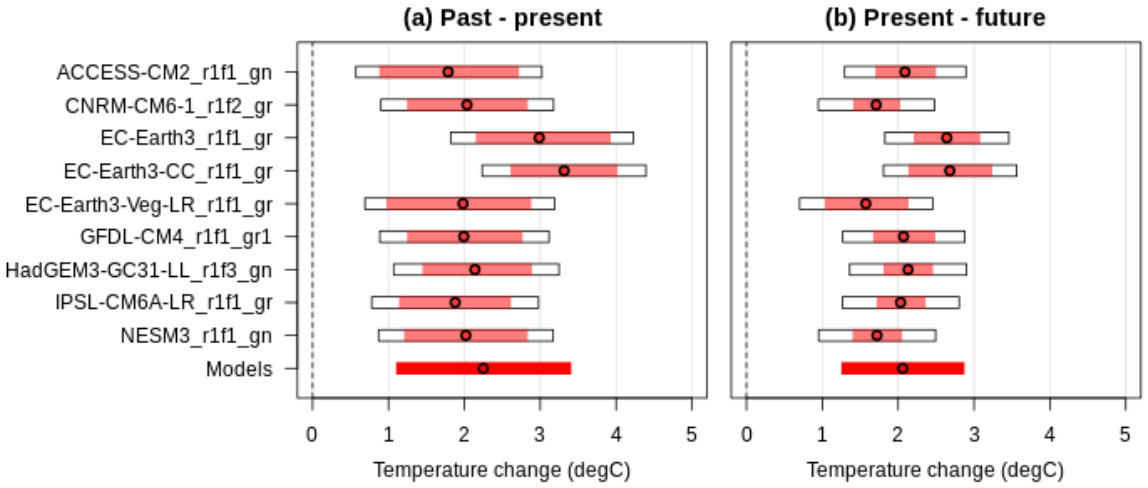

Figure A3.1: *Synthesis of change in intensity of Tx14x in Fennoscandia in the CMIP6 models when comparing (a) the 2025 climate and a 1.3°C cooler climate representing the preindustrial past and (b) the 2025 climate and a 1.3°C warmer climate representing the end of the century under current policies.*

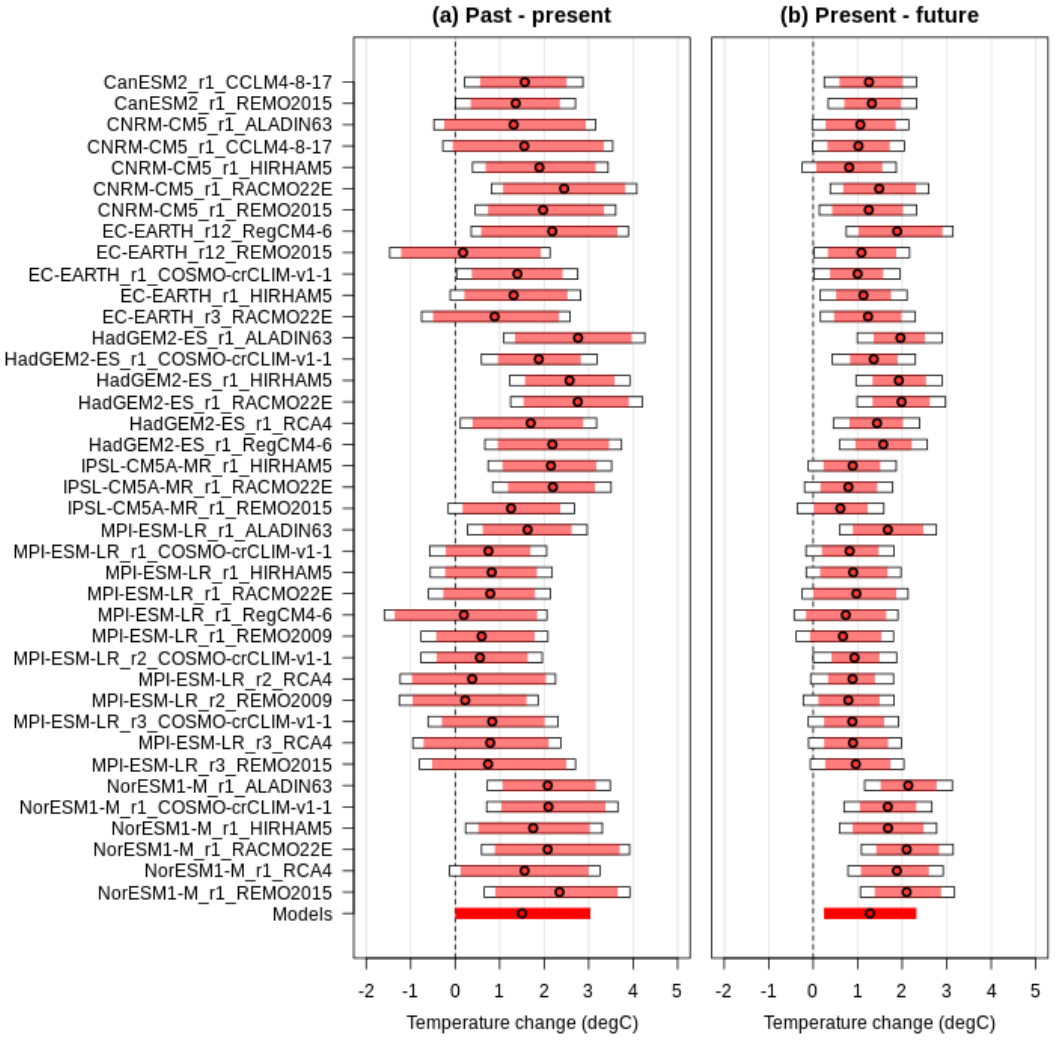

Figure A3.2: *As Figure A3.1, but for CORDEX models.*

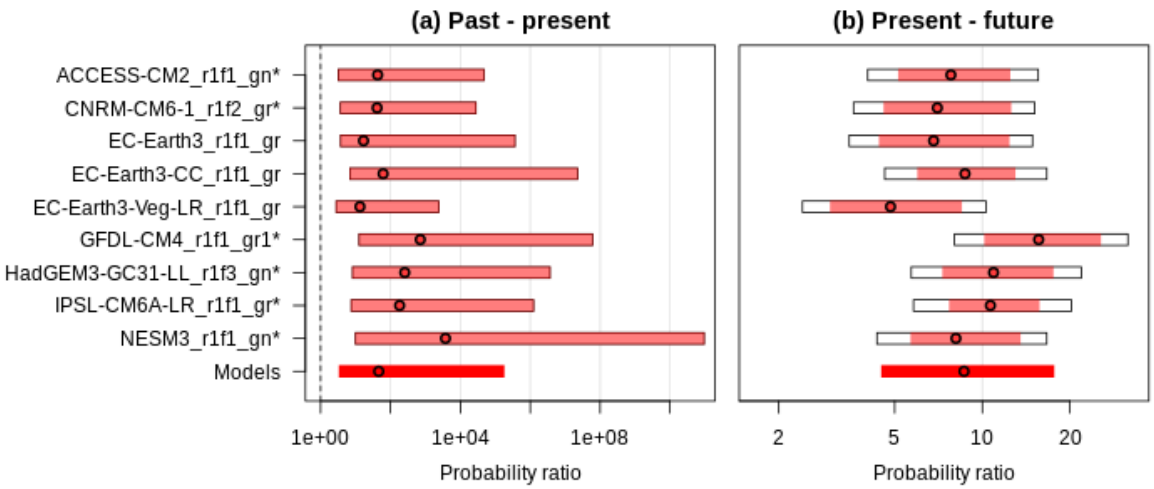

Figure A3.3: *Synthesis of change in likelihood of 1-in-50-year Tx14x in Fennoscandia in the CMIP6 models when comparing (a) the 2025 climate and a 1.3°C cooler climate representing the preindustrial past and (b) the 2025 climate and a 1.3°C warmer climate representing the end of the century under current policies.*

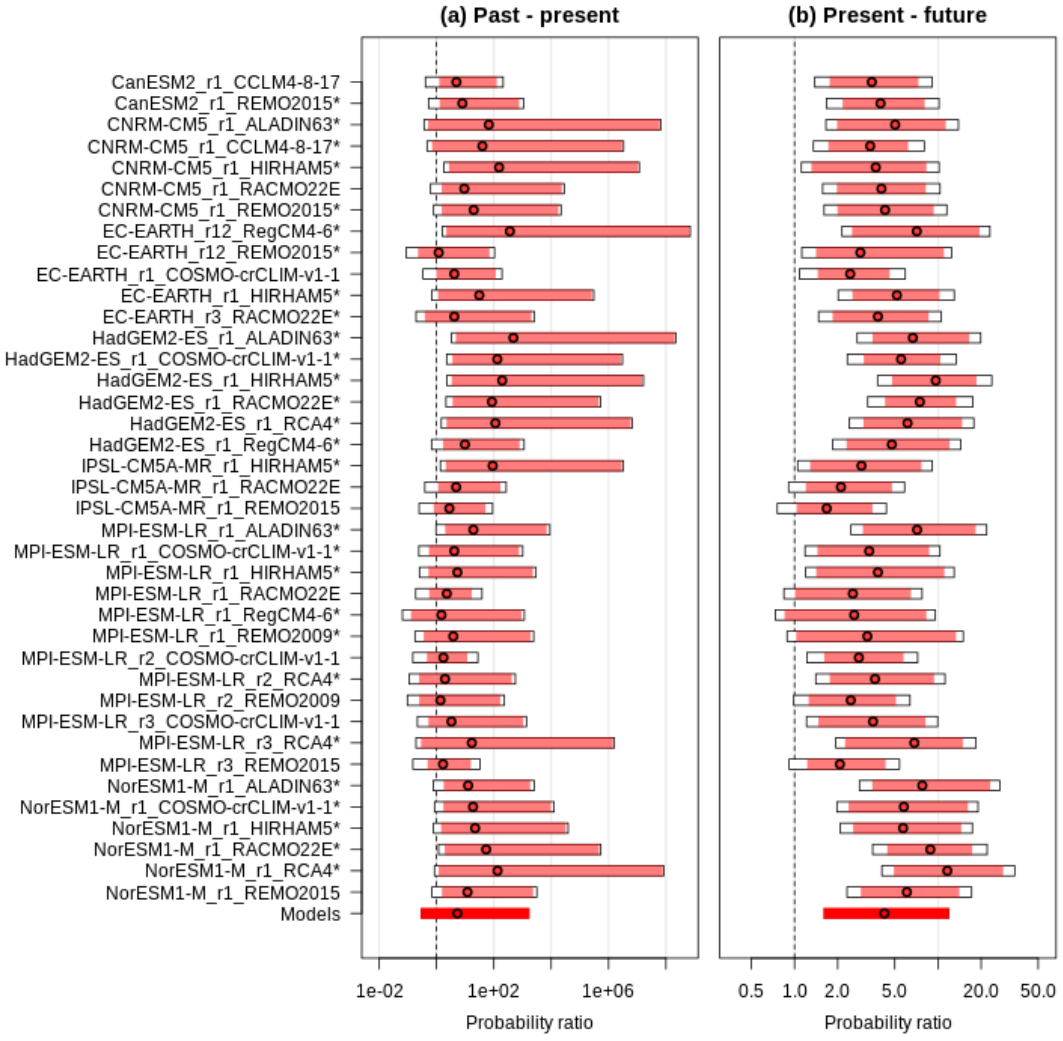

Figure A3.4: *As Figure A3.3, but for the Euro-CORDEX ensemble.*

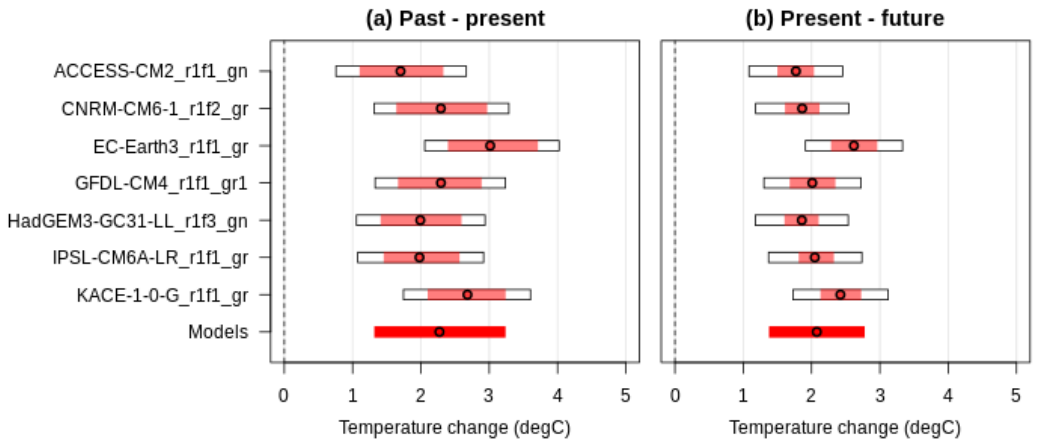

Figure A3.5: *Synthesis of change in intensity of Tn14x in Fennoscandia in the CMIP6 models when comparing (a) the 2025 climate and a 1.3°C cooler climate representing the preindustrial past and (b) the 2025 climate and a 1.3°C warmer climate representing the end of the century under current policies.*

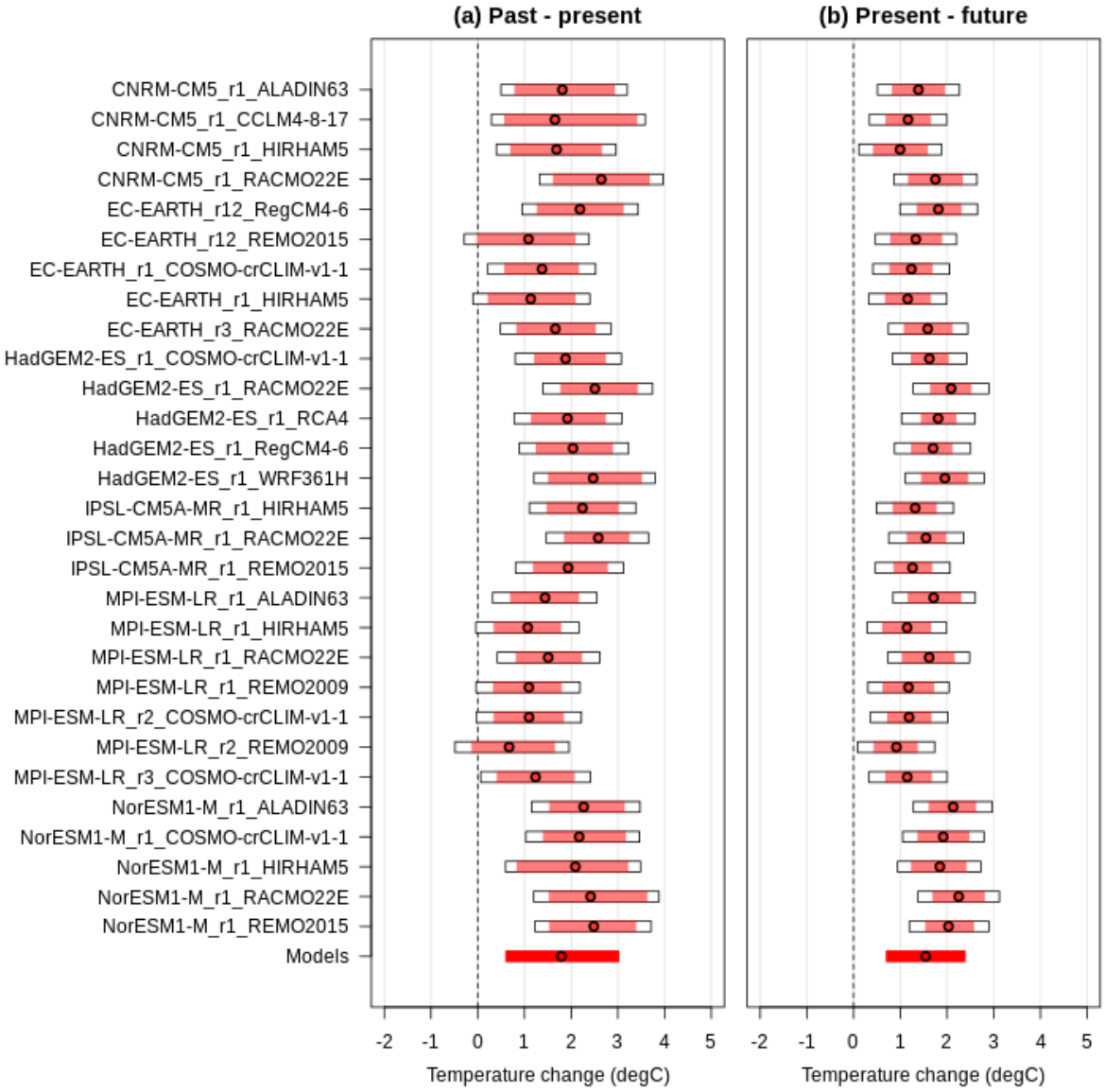

Figure A3.6: *As Figure A3.5, but for the Euro-CORDEX ensemble.*

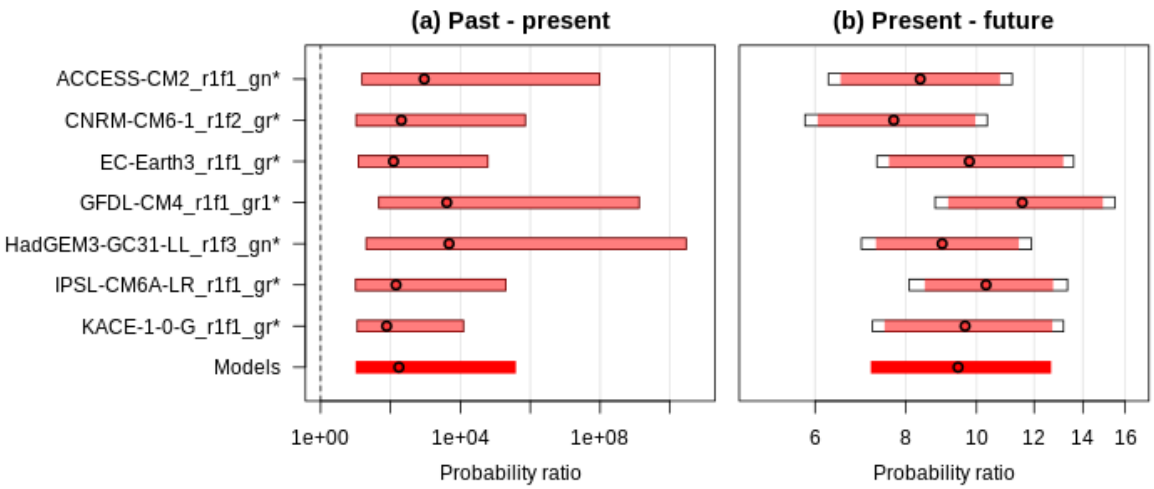

Figure A3.7: *Synthesis of change in likelihood of 1-in-20-year Tn14x in Fennoscandia in the CMIP6 models when comparing (a) the 2025 climate and a 1.3°C cooler climate representing the preindustrial past and (b) the 2025 climate and a 1.3°C warmer climate representing the end of the century under current policies.*

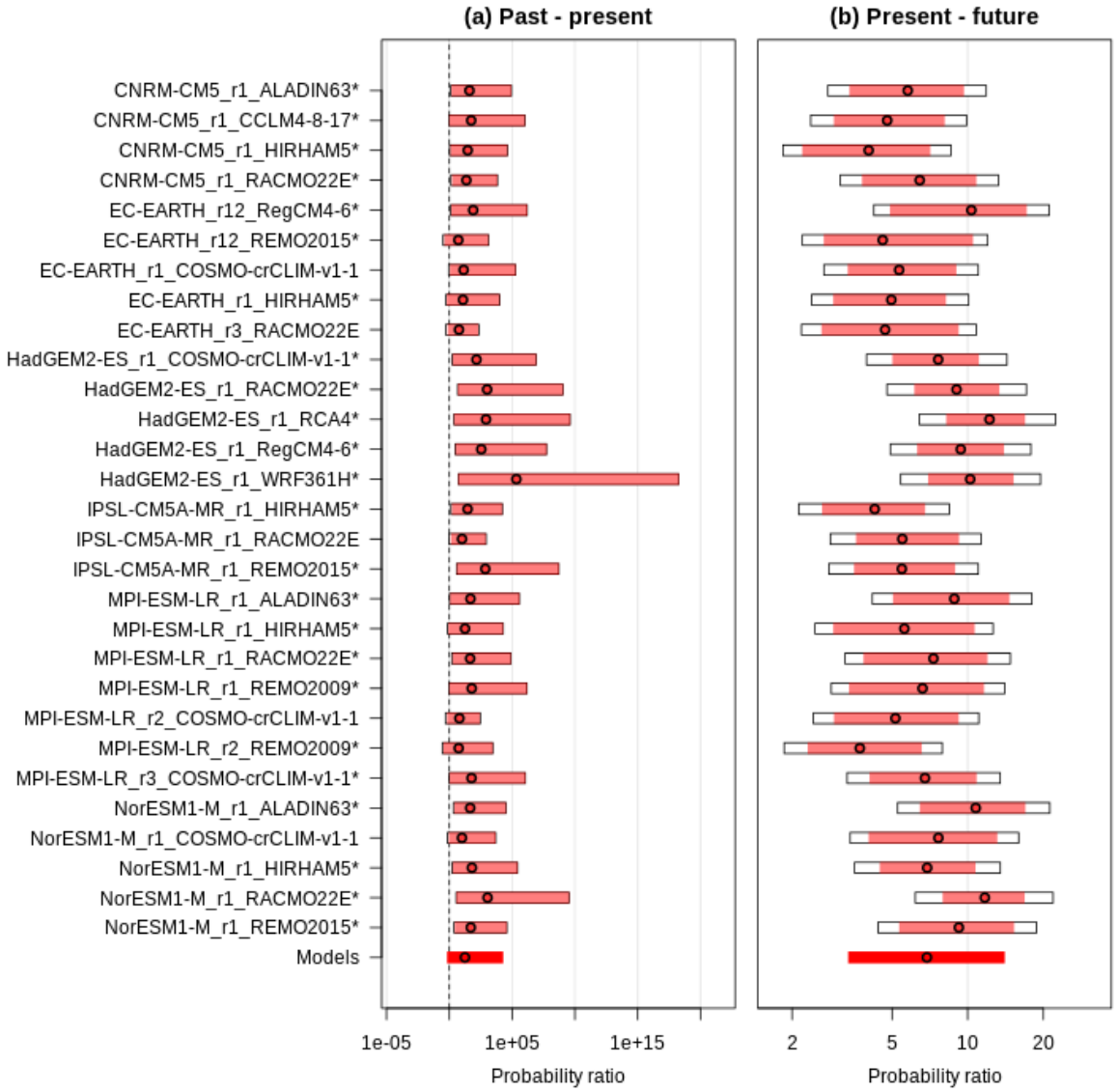

Figure A3.8: *As Figure A3.8, but for the Euro-CORDEX ensemble.*